Chapter 5

Targeting the tumor microenvironment via hierarchical disassembly of curcumin micelles: The pro-drug strategy

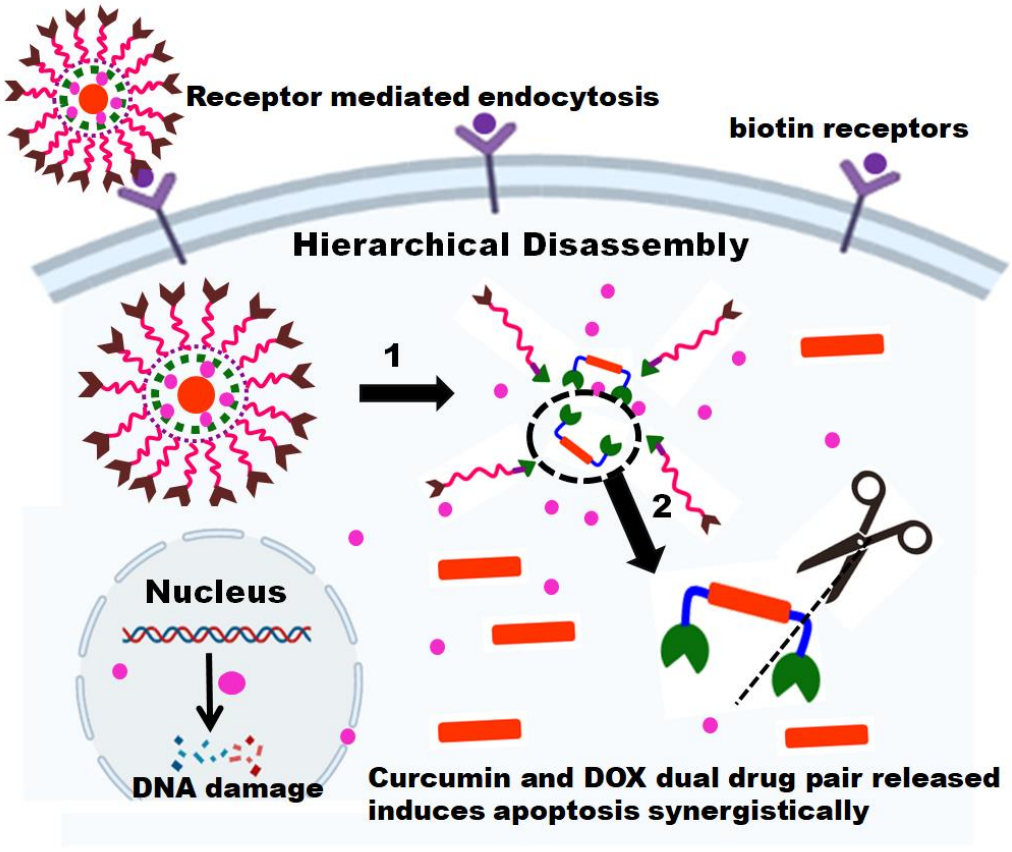

1. **Acetal Hydrolysis in acidic tumor microenvironment.**
2. **Intracellular enzymatic cleavage releasing curcumin from pro-drug.**

5.1 Introduction

The implementation of nanomedicine for overcoming challenges of cancer therapy has attained great impetus over the past few years. The administration of drug entrapped in rationally engineered carriers led to minimizing its systemic toxicity as compared to its bare counterparts[1]. Nanocarriers with targeting abilities can undergo by an accelerated tumor homing because of the enhanced permeability and retention (EPR) effect. Despite its successful application for tumor management, the bottleneck in efficiency of nanomedicines include encountering sequential drug delivery barriers, insufficient blood circulation process, in vivo rapid drug leakage, and limited tumor penetration capability [2,3]. A facile strategy to counter this paradox can be rational design of biocompatible nanocarriers undergoing self-adaptive transformations in terms of size selectively in tumor milieu like pH, enzyme, glutathione etc to release the cargo[4]. A structural metamorphosis in material microstructure only in the tumor microenvironment can be attained by introduction of acid labile ortho ester[5], hydrazone[6], cis-aconitic amide[7] and acetal linkages in it[8].

In particular, acetal bond has been explored by researchers in the past few years to assist an acid responsive hydrolysis of the carrier for accelerated drug release to cancer site. Towards this approach, the developments of pH sensitive drug loaded biodegradable nanostructures like micelles[9,10], vesicles[11,12], etc. has been reported to show superlative and selective delivery of drugs.

Another pressing issue of conventional drug delivery systems that has been a major concern for researchers is development of multidrug resistance (MDR). The multidrug resistant cancer cells function by overexpressing drug efflux pumps (like P-glycoprotein (P-gp)) on their surface which help to eliminate anticancer agents from cell environment[13,14]. Thus the drug loses its efficacy to destroy the tumor. Co-administration of a drug/agent that functions as a P-gp inhibitor along with a neoplastic drug can be an effective means for better treatment efficacy. The cocktail of anticancer drug and P-gp inhibitor acts by enhancing the penetration and accumulation of drug in the cancer cells. Naturally occurring curcumin is one such P-gp inhibitor that can not only suppress the P-gp expression but it also has the potential to down-regulate certain pathways (like PI3K/Akt and NF-kB) that generate physical obstruction for the drugs entering cancerous cells[15]. However, the extremely low solubility and poor stability of curcumin under physiological conditions has limited its bioavailability and therapeutic efficacy.

With this background, this work aims to develop curcumin pro-drug micelles that are as self-therapeutic in nature for addressing the above mentioned limitations of cancer therapy. The pro-drug micelles were formed by self-assembly of rationally synthesized block co-polymers. For the synthesis, curcumin was conjugated to a non-toxic pro-moiety (formyl benzoic acid) by ester linkage that improves its reactivity for incorporation into polymeric skeleton. This modified curcumin was then reacted with suitable molecules to introduce acetal and urethane linkages in the polymer. Such curcumin derived poly(acetal urethane) unit containing polymer was further conjugated with biotin tagged polyethylene glycol polymer. Polyethylene glycol was utilized with the aim of improving the blood circulation time of the carrier. Biotin tagging was done to endow the resulting micelles with the property of receptor mediated endocytosis. Vitamins are well-known to selectively target cancer cells[16,17]. Biotin or Vitamin-H also known as B7 is an essential nutrient for the growth of cancer cells. Thus vitamin-H receptors are overexpressed on the surface of cancer cells.

The amphiphilic copolymer has the capability to self-assemble into stable micelles in aqueous media. It is noteworthy that the amphiphiles contain both acid responsive acetal groups and enzyme sensitive ester linkage. The acetal groups are insensitive to presence of enzyme whereas the ester linkage is insensitive towards pH changes and hence the micelle is expected to undergo a hierarchical degradation in the tumor microenvironment. The micelle formation, pH responsive degradation of the polymer via acetal hydrolysis and enzyme responsiveness was studied in detail. The interior of micelles was used to load the well-known anticancer drug doxorubicin (DOX) and the release profiles under mimicked conditions were assessed. Since the micelles are polymeric nanocarriers, they have the ability of passive targeting by enhanced permeability and retention effect and further biotin tagging introduces active and selective targeting. To the best of our knowledge, such hierarchically disassembling, dual responsive doxorubicin loaded curcumin prodrug micelle targeting liver cancer cell lines via biotin has not been reported so far. The combination index was also calculated to ascertain the cocktail of DOX and curcumin being used for the treatment exerts a synergistic effect. For comparison a similar curcumin derived non-responsive carrier was synthesized and its assessment as a drug carrier was made. The benefits of having stimuli response in a drug carrier has been shown from the results of the comparative study. The efficacy of both responsive and non-responsive carriers was to act as potential

materials for tumor homing was evaluated both in-vitro on HepG2 cell lines and in-vivo on nude mice model.

5.2 Experimental Section

5.2.1 Materials

Curcumin (99.0%), Polyethylene glycol (PEG, Mn = 2.0, 4.0 and 6.0 kg/mol), hexamethylene diisocyanate (HMDI), biotin (99%) and 1,4-diazabicyclo[2.2.2]octane (DABCO) and phosphate buffer saline tablets (for preparation of pH 7.4 buffer solution) were purchased from Sigma Aldrich. Sodium acetate, acetic acid, sodium hydroxide, hydrochloric acid for preparation of other buffers of pH 4.0 and 5.0 were received from Sisco Research Laboratories (SRL), India. 4-Formylbenzoic acid (FBA) (98%), 1,1,1-tris(hydroxymethyl)ethane (TME) (99%) and p-toluenesulfonic acid (PTSA) (99%) were procured from Spectrochem India. Doxorubicin hydrochloride (DOX·HCl) (99%) was ordered from Sigma Aldrich. Various solvents viz. toluene, N,N,- Dimethylformamide (DMF), Dimethylsulfoxide (DMSO), acetone, dichloromethane (DCM) were obtained from SRL. Other reagents were of analytical grade, purchased from commercial sources and used as received without further purification. The solutions were prepared using de-ionized water.

5.2.2 Characterization

Nuclear magnetic resonance (^{1}H NMR) studies were performed on a Bruker Avance 400 MHz spectrometer using DMSO-d^6 or $CDCl_3$ as solvents and tetramethylsilane as an internal standard. Fourier transform infrared spectroscopy (FTIR) measurements were performed on Bruker Alpha IR spectrophotometer. The samples were ground with KBr and turned into pellets by disc pressing. The spectra were recorded in 400-4000 cm^{-1} range. The molecular weight and polydispersity index of the polymers was determined using Agilent 1260 II Gel permeation chromatography (GPC) instrument using a 2* Mixed-B column protected with a guard column. The instrument was equipped with a refractive index (RI) detector. 0.2% LiBr in DMF was used as an eluent at a flow rate of 0.75 ml/min, the oven temperature was maintained at 40°C. For high resolution transmission microscopy (HR-TEM) determinations, diluted polymer and DOX loaded polymer solutions were dispersed on carbon coated copper grids. The sample coated grids were then air dried overnight under ambient temperature. The imaging was then recorded on a

Jeol (Jem-2100F) electron microscope at an accelerating voltage of 200 kV. Dynamic light scattering (DLS) was used to determine the hydrodynamic diameter and polydispersity of micelles in the solution which was performed on Beckman Coulter Delso Nano. AFM and FE-SEM were recorded on NTEGRA PRIMA, NT-MDT, Russia and JSM7600F respectively. UV-vis spectrophotometric determinations were done using Perkin Elmer Lambda 35 and Fluorescence spectra were scanned on JASCO FP-6300.

5.2.3 Synthesis of curcumin derived amphiphilic polymers

5.2.3.1 Synthesis of Curcumin-Aldehyde (CUR-ALD)

4-Formylbenzoic acid (2.33 g, 15.5 mmol) was dissolved in 10 ml of dichloromethane (MDC) pre-cooled at 0-5 °C. To this mixture, 1-Ethyl-3-(3-dimethylaminopropyl) carbodiimide hydrochloride (EDC.HCl) (2.33 g, 12.15 mmol) was added and the resulting solution was stirred for 90 minutes. This is followed by the addition of curcumin (1.0 g, 2.75 mmol) and dimethylaminopyridine (DMAP) (0.25 g, 2.04 mmol) to the reaction mass. Post this addition, the temperature of the reaction mass was increased to room temperature and continued for 24 h at 30 °C. The reaction was continuously monitored by TLC using (1:1) ethyl acetate and petroleum ether as the solvent system. The product precipitates as yellow solid and was separated by vacuum filtration. The product was further given washings of cold water to remove unreacted EDC and DMAP followed by washings of diethyl ether for purification. The purified product was stored in vacuo until further use. (Yield 88 %, melting point 218°C)

^{1}H NMR (400 MHz, $CDCl_3$): δ (ppm): 9.89 (1H, -CHO), 8.04, 8.06 (2H; 1 -C (=O), 1 -C=O), 8.39, 8.41 (2H; 1 -C (=O), 1 -C=O) protons of FBA, 7.21, 7.23, 7.24 (3H, -CH aromatic protons of curcumin), 7.67, 7.71 (1H, curcumin), 3.90 (3H, $-CH_3$), 4.59 (1H, $-CH_2$)

FTIR (KBR pellet): wavenumber (cm^{-1}) 1740 (C=O of ester), 1230 (C-O of ester), 1685 (C=O of aldehyde), 2525, 3023 (C-H stretch aromatic)

5.2.3.2 Synthesis of Curcumin-acetal linkage containing moiety (CUR-ACET)

Aldolization reaction was carried using CUR-ALD and TME as the reactant to synthesize of CUR-ACET. Briefly CUR-ALD (0.5 g, 0.79 mmol), PTSA (0.25 g, 1.45 mmol), and TME (2.5 g, 20.80 mmol) were dissolved in 80 mL toluene. The resulting reaction mixture was stirred at

120 °C for 8 h. The progress of reaction was monitored by TLC using 1:1 mixture of ethyl acetate and petroleum ether as solvent system. After 8h the reaction mass was concentrated by evaporation and the residue obtained was given washings of 10 mM phosphate buffer of pH 7.4. The product was filtered and dried under vacuum for 48 h. (Yield 83%, melting point 202°C)

^{1}H NMR (400 MHz, DMSO-d^6): δ (ppm): 8.13, 7.62 (-CH) protons of FBA, 5.98 (-CH of acetal linkage), 3.81 and 3.55 (-CH_2 of acetal linkage), 4.24 (free -OH of TME), 0.89 (-CH_3 of TME) 7.18, 7.30, 7.37 (3H, -CH aromatic protons of curcumin), 6.91, 7.60 (1H, curcumin), 3.87 (3H, -OCH_3), 4.59 (1H, -CH_2).

FTIR (KBR pellet): wavenumber (cm^{-1}) 1746 (C=O of ester), 1233 (C-O of ester), 3021 (C-H stretch aromatic), 1395 (O-CH-O, acetal linkage)

5.2.3.3 Synthesis of PEGylated biotin polymer

Biotin was reacted with PEG_x by esterification reaction. PEG of varying molecular weights were selected (Mn= 2000 g/mol, 4000 g/mol and 6000 g/mol) to prepare 3 different polymers. Briefly for the reaction, biotin (0.0488 g, 0.20 mmol; 0.029 g, 0.12 mmol and 0.020 g, 0.083 mmol) and PEGx (0.5 g, 0.20 mmol, 0.12 mmol and 0.083 mmol respectively) were dissolved in DMF. DCC (0.1 g, 0.48 mmol) and DMAP (0.05 g, 0.41 mmol) were added to this mixture. The reaction mass was allowed to stir at 30 °C for 24 h. After 24 h, the reaction mixture was vacuum filtered to ensure the removal of DCU and unreacted reagent. The product was precipitated from this solution using diethyl ether. The product was separated by vacuum filtration and stored under vacuum until further use. (Yield 85 %)

^{1}H NMR (400 MHz, DMSO-d^6): δ (ppm): 6.38, 6.46 (1H, -NH), 4.30, 4.32 (1H –CH), 1.06, 1.08, 1.10 (4H, -CH_2), 2.1 (-CH), 3.64, 3.62 (1H, -OCH_2 characteristic peak of PEG) 4.59 (1H, -OH)

FTIR (KBR pellet): wavenumber (cm^{-1}) 1105 (C-O of ester), 1737 (C=O of ester), 3310 (-OH of PEG), 2931, 1020, 1481 (characteristic peaks of biotin)

5.2.3.4. Synthesis of biotin tagged acetal/ester linkage containing amphiphiles

The biotin targeting responsive amphiphiles were prepared via polycondensation of CUR-ACET and PEGylated biotin using HMDI as the linker. The three different PEGylated biotin polymers

P1, P2 and P3 having varying Mn of PEG were linked to the CUR-ACET fragments to form 3 different amphiphiles. The amphiphiles were designated as B-CUR-(A)-P1, B-CUR-(A)-P2and B-CUR-(A)-P3, where P1 contains PEG_{2000}, P2 has PEG_{4000} and P3 has PEG_{6000} respectively. Briefly, HMDI (0.168 g, 1.0 mmol) was added to a solution of CUR-ACET (0.795 g, 0.95 mmol) and PEGylated biotin (0.05 g) in DMF (5.0 mL). DABCO (5.0 mg) was added a catalyst and the reaction was allowed to proceed at 60 °C for 6 h. The resulting polymer was precipitated as yellow solid using diethyl ether and purified thrice by dissolving in DMF and re-precipitation in diethyl ether. The purified polymer was filtered and dried in vacuo and stored under vacuum until further use. Yield: 70 %.

^{1}H NMR (600 MHz, DMSO-d^6) δ (ppm): 8.13, 7.62 (-CH) protons of FBA, 5.98 (-CH of acetal linkage), 3.81 and 3.55 (-CH_2 of acetal linkage), , 0.89 (-CH_3 of TME), 7.18, 7.30, 7.37 (3H, -CH aromatic protons of curcumin), 6.91, 7.60 (1H, curcumin), 3.87 (3H, -OCH_3), 4.59 (1H, -CH_2), 6.38, 6.46 (1H, -NH), 4.30, 4.32 (1H –CH), 1.06, 1.08, 1.10 (4H, -CH_2), 2.1 (-CH), 3.64, 3.62 (1H, -OCH_2 characteristic peak of PEG), 7.01 (-NH of urethane), 1.43, 1.62, 3.3 (-CH_2 protons of HMDI).

5.2.3.5. Synthesis of biotin tagged nonresponsive amphiphile

The mono-acetyl curcumin was synthesized as per previously reported procedure[18]. Briefly, HMDI (0.168 g, 1.0 mmol) was added to a solution of acetylated curcumin (0.389 g, 0.95 mmol) and PEGylated biotin (0.05 g) in DMF (5.0 mL). DABCO (5.0 mg) was added a catalyst and the reaction was allowed to proceed at 60 °C for 6 h. The resulting polymer was precipitated as yellow solid using diethyl ether and purified thrice by dissolving in DMF and re-precipitation in diethyl ether. The purified polymer was filtered and dried in vacuo and stored under vacuum until further use. Yield: 70 %. This amphiphile was designated as **B-CUR-P4**

^{1}H NMR (600 MHz, DMSO-d^6) δ (ppm): 7.18, 7.30, 7.37 (3H, -CH aromatic protons of curcumin), 6.91, 7.60 (1H, curcumin), 3.87 (3H, -OCH_3), 4.59 (1H, -CH_2), 6.38, 6.46 (1H, -NH), 4.30, 4.32 (1H –CH), 1.06, 1.08, 1.10 (4H, -CH_2), 2.1 (-CH), 3.64, 3.62 (1H, -OCH_2 characteristic peak of PEG), 7.01 (-NH of urethane), 1.43, 1.62, 3.3 (-CH_2 protons of HMDI)

5.2.4 Formation of micelles via self-assembly of amphiphiles and determination of its critical micelle concentration (CMC)

The micelles were prepared from amphiphiles by solvent exchange method. Briefly 1.0 mL of the amphiphilic polymers of 10 mg/ml concentration was added dropwise into a solution of 0.9 mL of PBS buffer pH 7.4. The solution was left for stirring at 37°C for 1 hour and then subjected extensive dialysis against PBS buffer 7.4 using a dialysis membrane of molecular weight cutoff (MWCO) of 3500 Da. The critical micelle concentration (CMC) was obtained by fluorescence spectrophotometry employing pyrene as a probe. For determination of CMC, 1.0×10^{-5} mg/ml to 0.1 mg/mL concentration of the polymer were used was varied from whereas the concentration of pyrene was fixed at 1.0×10^{3} M. The fluorescence spectra were then recorded at an excitation wavelength of 330 nm. The emission fluorescence at 370 and 385 nm was monitored. The point of intersection on extrapolating the intensity ratio I_{370}/I_{385} in the high and low concentration regions was designated as the CMC value.

5.2.5 Study of pH-triggered hydrolysis of the acetal linkage in micelles

The hydrolysis of the acetal linkages in all the acetal linkage polymers was determined with the help of UV-vis spectroscopic measurements at 430 nm. The micellar solutions were prepared at 1.0 mg/mL concentration and divided into three aliquots. The pH of these 3 aliquots was attuned to pH 4.0, 5.0, and 7.4 via addition of 40 μL of pH 4.0 and 5.0 acetate buffer or pH 7.4 PB, respectively and maintained at 37 °C. The aliquot 100 (μL) was taken out at predefined time intervals, and diluted using 3.0 mL of PBS buffer, pH 7.4). The absorbance of aliquots was measured at 430 nm. To ensure complete hydrolysis, concentrated HCl was added to all the samples and the absorbance of this solution at 430 nm was noted used to quantify the acetal hydrolysis.

5.2.6 Assessment of pH responsive degradation of curcumin prodrug micelles

The extent of acetal hydrolysis in micelles was monitored using UV-vis spectroscopy. The micellar solutions were prepared by using 1 mg/ml polymer and separated as three different aliquots. The pH of these three solutions were adjusted to pH 7.4, 5.0 and 4.0 using phosphate and acetate buffers respectively and incubated at 37 °C. At predetermined time intervals, 100 μL of aliquot was removed and diluted with 3.0 mL of PBS buffer pH 7.4. The absorbance of this

solution was then measured at 430 nm. Finally, all the samples were subjected to complete hydrolysis by addition of concentrated HCl and the acetal hydrolysis was quantified by measuring the absorbance at 430 nm.

5.2.7 Monitoring size of the change of acetal linkage containing micelles in response to acidic pH

The changes occurring in size as well as size distribution in response to various acidic pH values were measured using. For this, 1.0 mL of micellar dispersions (0.5 mg/mL) were prepared as mentioned above and maintained at 37 °C and was added 40 μL of acetate buffer (4 M, pH 5.0). The changes in micellar size were analyzed via DLS.

5.2.8 Drug Loading and Release Studies.

Firstly, DOX.HCl was stirred with 2 molar equivalent of triethylamine in DMSO overnight for removal of HCl [19].

5.2.8.1 Loading of DOX. The desalted DOX-loaded micelles were prepared via dropwise addition of 1.0 mL of PBS (pH 7.4) to a 100 μL solution of copolymer in DMF having 10 mg/mL concentration. DOX solution in DMSO 25 μL, having 5 mg/mL concentration was mixed with the above mentioned solution and stirred at room temperature. The resulting solution was dialyzed against 10 mM phosphate buffer using a dialysis bag with MWCO of 3500 extensively for 12 h. The dialysis media was repeatedly changed thrice.

The process of loading was carried out under dark. The amount of DOX was determined by a UV-visible spectrophotometer with at 480 nm. For determination of the drug loading content (DLC), the lyophilized DOX-loaded micelles were re-dissolved in DMSO and analyzed with UV spectroscopy. The calibration curve was constructed by using solution of DOX in DMSO having different concentrations. DLC and drug loading efficiency (DLE) were calculated according to the following formula:

DLC (%) = [weight of drug in carrier/weight of carrier taken] ×100 ------ (1)

DLE (%) = [weight of drug in carrier/ weight of drug in feed] ×100 ------ (2)

5.2.8.2 Acid-Triggered Release of DOX and Curcumin

The drug release from DOX-loaded micelles was investigated at 37 °C in three different media, i.e., 10 mM acetate buffer having pH 4.0, 10 mM acetate buffer having pH 5.0, and 10 mM phosphate buffer having pH 7.4. The DOX-loaded micelles of 0.1 mg/mL concentration were then split into three aliquots of 0.5 mL each. The solutions were then transferred to a dialysis bag with a MWCO of 12000 Da. The dialysis bag was then placed into 25 mL of corresponding buffer solutions under test at 37 °C. 5 mL of release media was taken out at predetermined time interval and replenished with same volume of fresh media. For the determination of DOX release, calibration curves were plotted in corresponding buffer solution. The experiments were carried out thrice and average values were reported.

To monitoring the drug release under enzymatic conditions, similar protocol was followed by addition of 5 U of esterase enzyme in the dialysis bag (MWCO 1.0 KDa). The percentage cumulative release of drug was calculated as per the equation mentioned below.

$$\boldsymbol{Cumulative\ drug\ release} = \frac{\boldsymbol{Amount\ of\ drug\ released\ in\ time\ 't'}}{\boldsymbol{Total\ amount\ of\ drug\ in\ carrier\ taken\ in\ dialysis\ bag}} \times \mathbf{100} \quad \textbf{-- (3)}$$

Similarly drug release in FBS at 37 °C was also carried out to assess the release from carriers under physiological conditions.

5.2.9 In-vitro Studies

Cell Culture and Cell Viability assay

The studies were carried on cancerous HepG2 (Human hepatocellular carcinoma cell Line) and healthy NIH 3T3 fibroblasts. The cell lines were procured from National Centre of Cell Sciences, Pune, India and treated and maintained as per the protocol mentioned in previous chapters. The obtained values of cell viability are plotted against the concentration of drug, micelles and drug loaded micelles.

Similarly the cellular internalization were performed by dosing both cancerous and normal cells with fluorescein loaded micelles and incubated for 4 h and later photographed using a

fluorescence microscope. Cell viability studies were performed by PI staining technique on the HEPG2 cell lines

5.2.10 In-vivo Studies

Balbc mice were used as for the studies and distributed into various treatment groups as follows; For the experiment, animals were divided in 7 treatment groups as follows with n=6 mice per group. The animals in group 1(G1) were dosed only with double distilled water and designated as control group. The physiological parameters determined from this group were considered as the standard values for cancer free condition. The animals in the remaining groups (G2 to G7) were administered with HepG2 cells intraperitoneally to induce hepatic tumor (HCC). After the successful tumor induction, animals of group 2 (G2) were dosed with only PBS and designated as untreated group. The treatment groups consisted of group 3 (G3) dosed only with DOX, group 4 (G4) dosed with B-CUR-(A)-P3 (biotin tagged self-therapeutic micelles, which are both enzyme and pH responsive) group 5 (G5) injected with B-CUR-P4 (biotin tagged non-responsive micelles), group 6 (G6) administered with DOX loaded B-CUR-(A)-P3 (10 mg kg^{-1}) and group 7 (G7) treated with DOX loaded B-CUR-P4.

Various qualitative and quantitative parameters selected for demonstrating the anticancer potential of the drug loaded carriers were as per mentioned in previous chapters.

5.2.11 Statistical analysis

All experiments have been performed at least in triplicate and expressed as means ± standard deviation (SD). The differences among groups were analyzed using the paired, two-sided Student's t-test. P-value < 0.05 were considered significant, and P-value < 0.01 were considered to be highly significant.

The detailed protocol for preclinical studies have been mentioned in the supplementary information.

5.3 Result and Discussion

5.3.1 Synthesis of various curcumin derived amphiphilic polymers

The biotin tagged, curcumin derived, dual responsive amphiphilic copolymers were synthesized as depicted in **Scheme 5.1**. The first step in preparation of amphiphile involves synthesis of

curcumin prodrug by employing formyl benzoic acid as a pro-moiety. The synthetic strategy involves conjugation of both the components by an ester linkage that can be undergo cleavage on exposure to enzymes present in the intracellular compartments.

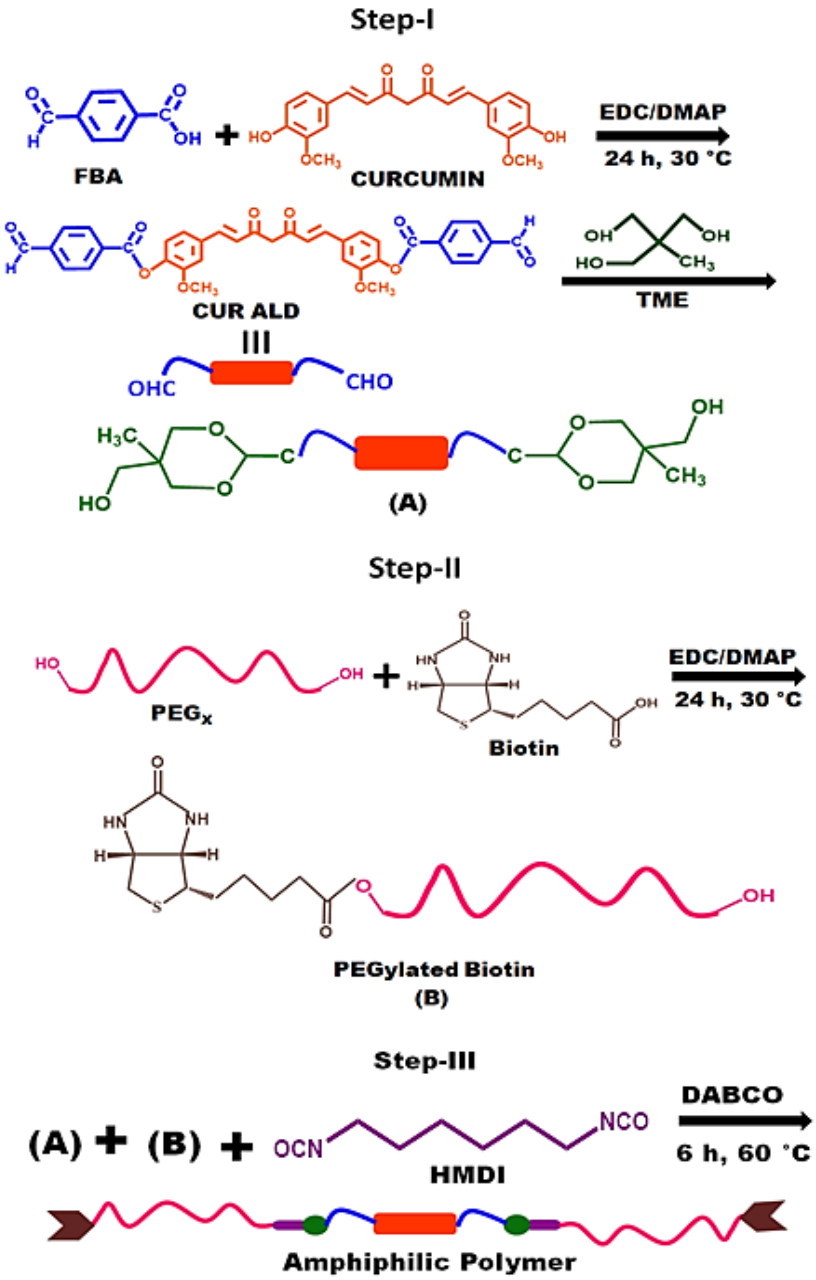

Scheme 5.1: Synthetic route for preparing biotin tagged, acetal and ester linkage containing; pH, enzyme dual responsive amphiphilic polymer capable of self-assembling into prodrug micelle.

Curcumin and formyl benzoic acid were reacted by esterification using EDC-DMAP. The successful esterification is confirmed by the disappearance of the peak corresponding to hydroxyl groups of curcumin that usually appears around 16 ppm. Further the appearance of peak at 9.89 ppm corresponding to free CHO groups from formyl benzoic acid unit, confirms the formation of the desired curcumin-aldehyde product (CUR-ALD) **(figure 5.1)**.

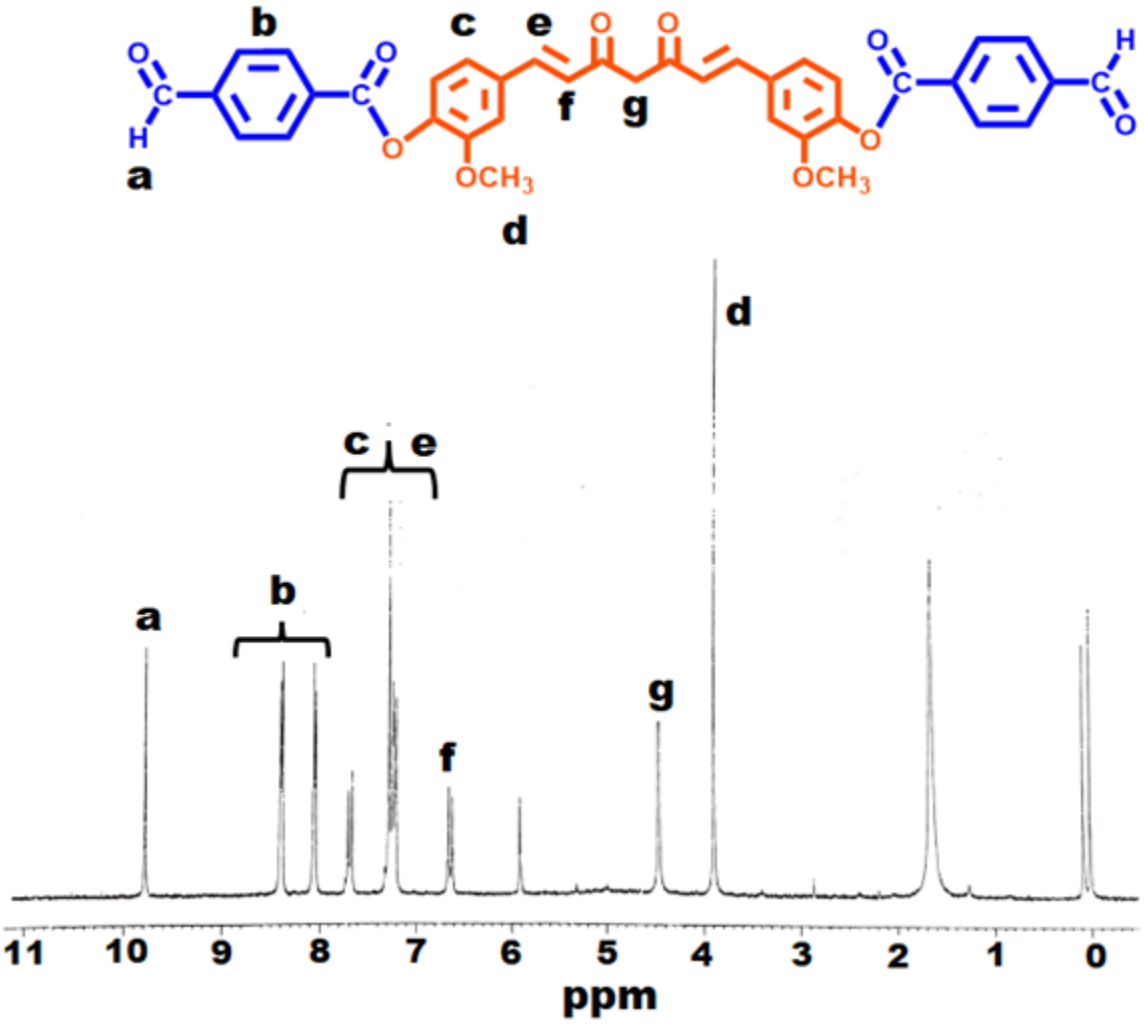

Figure 5.1: ^{1}H NMR of curcumin modified with 4-formylbenzoic acid (CUR-ALD)

The free aldehyde groups from this unit were further used for aldolization reaction for introduction of diacetal groups in the polymer backbone **(figure 5.2)**. The reaction of CUR-ALD and TME with catalytic quantity of PTSA yielded CUR-ACET **(designated as 'A' in scheme 1).** The incorporation of this fragment in the final polymer leads to its acid responsiveness.

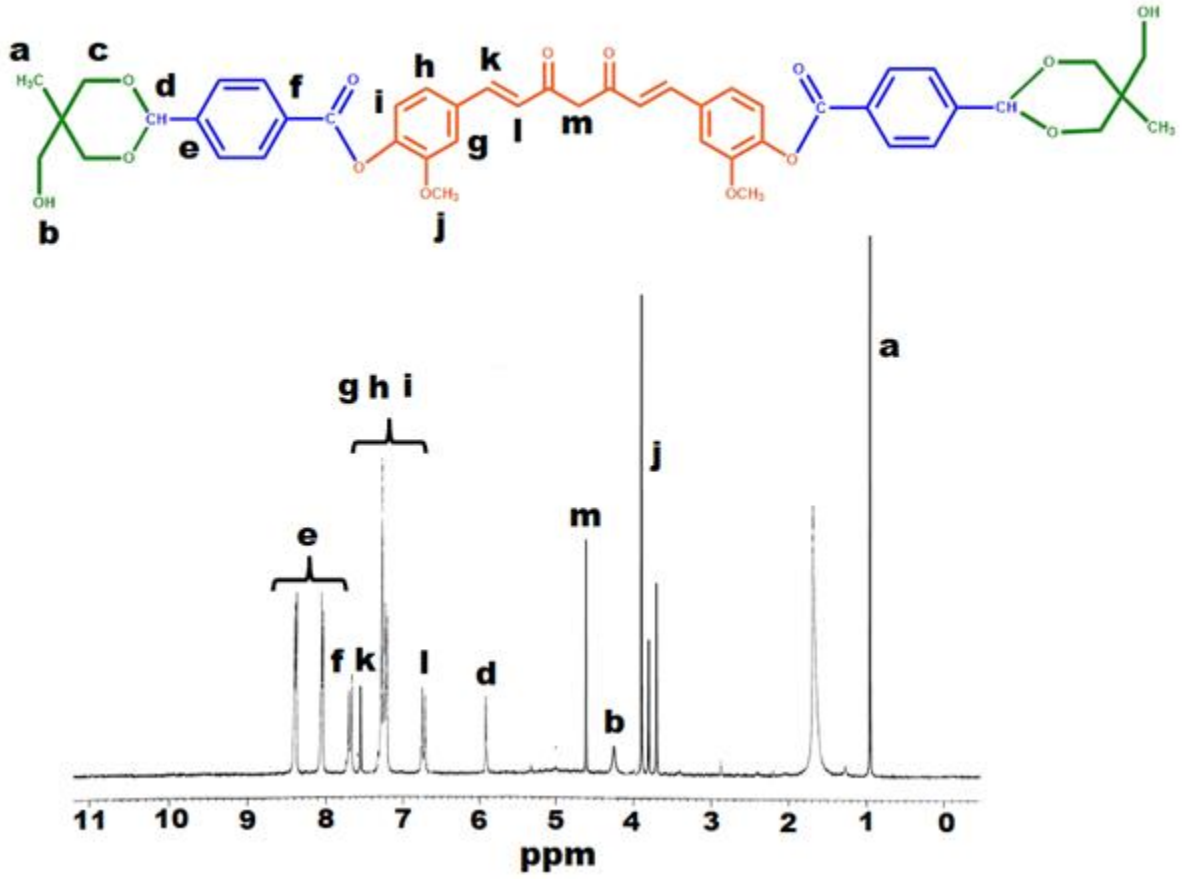

Figure 5.2: ^{1}H NMR of aldolization product (CUR-ACET)

For biotin conjugation with PEG_X, esterification with facile DCC chemistry was carried out. The appearance of peak corresponding to proton of -NH group at 6.38 ppm of biotin in addition to the characteristic $–OCH_2$ peak of PEG at 3.64 ppm confirmed the reaction of both the reactants **(figure 5.3)**. The product is designated as **B** in **scheme 1**.

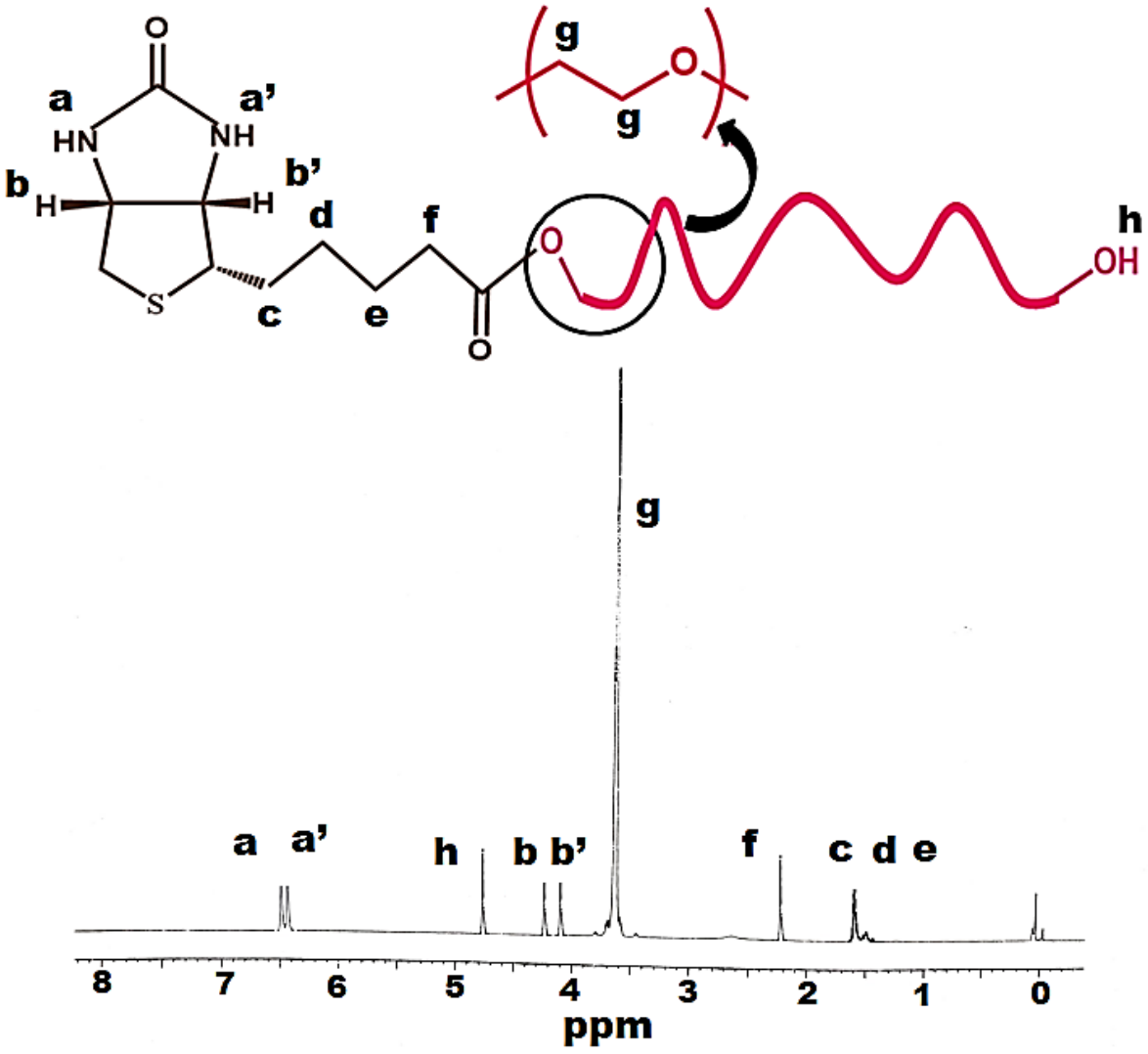

Figure 5.3: ^{1}H NMR of pegylated biotin.

The final amphiphile was obtained by polycondensation reaction, using HMDI as a linker to attach both pre-polymers **A** and **B.** The conjugation is established as urethane proton appeared at 7.01 ppm in addition to the characteristic protons of other constituent units supporting the formation of desired polymer **(figure 5.4)**.

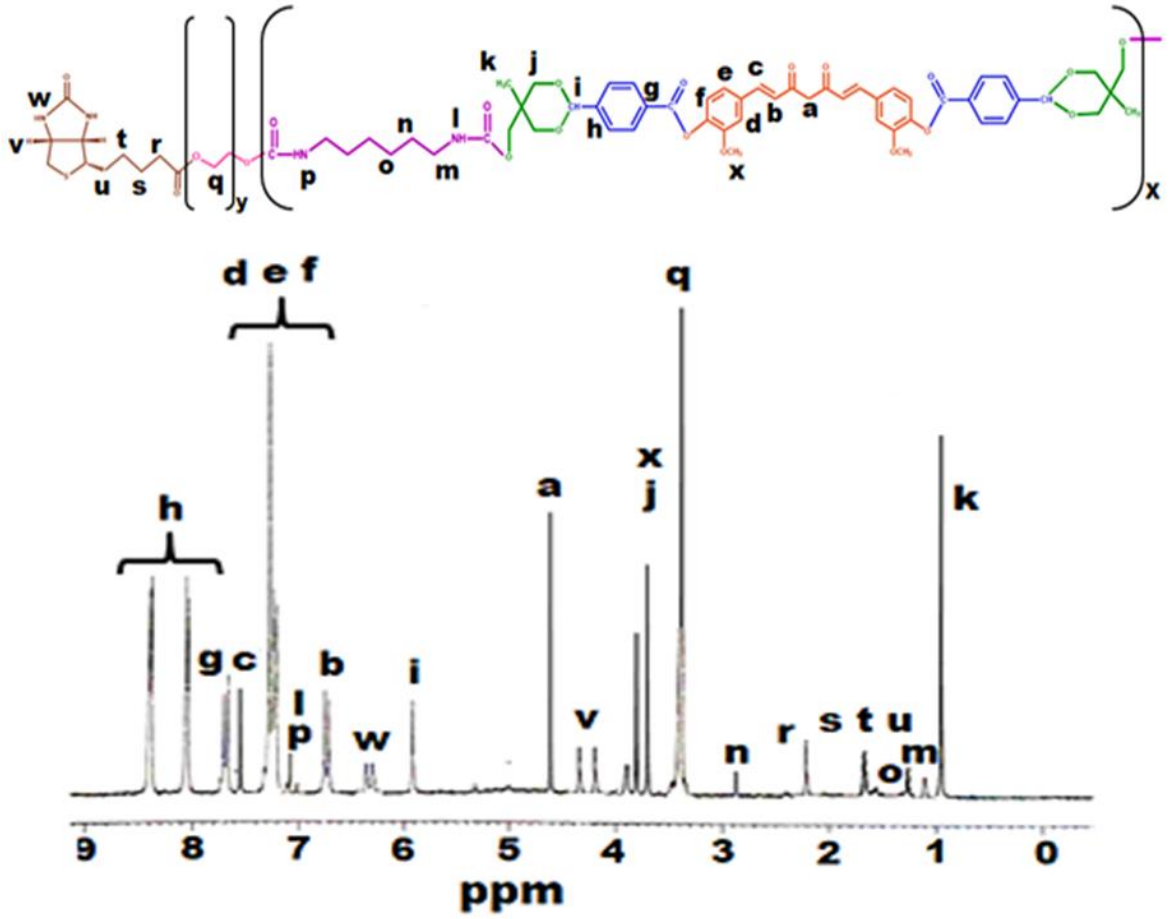

Figure 5.4: ^{1}H NMR of biotin tagged curcumin derived amphiphilic block co-polymers B-CUR-(A)-P1-P3

For comparison as well as to understand the effect and importance of stimuli responsiveness in targeted drug delivery another curcumin derived amphiphile using similar components was synthesized **(scheme 5.2)**. However this polymer is devoid of any stimuli responsive groups **(figure 5.5)**.

The FTIR spectra overlay **(figure 5.6)** also suggests the modifications in the polymer structure

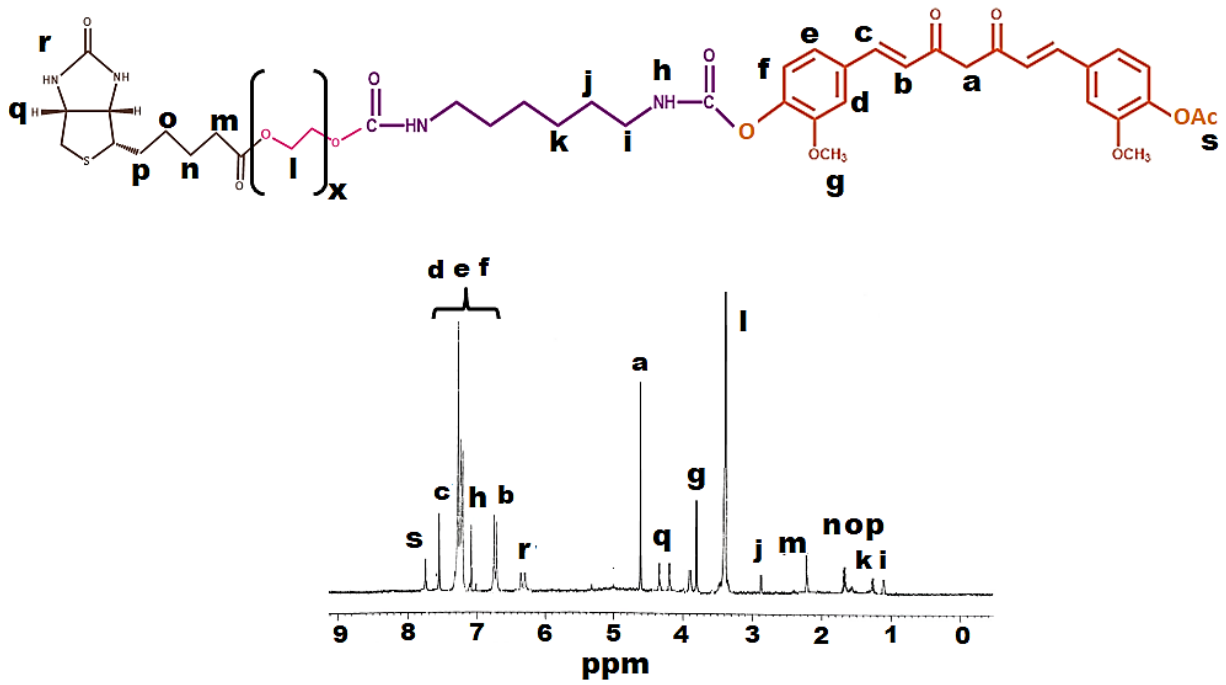

Figure 5.5: ^{1}H NMR of non-responsive amphiphile (B-CUR-P4)

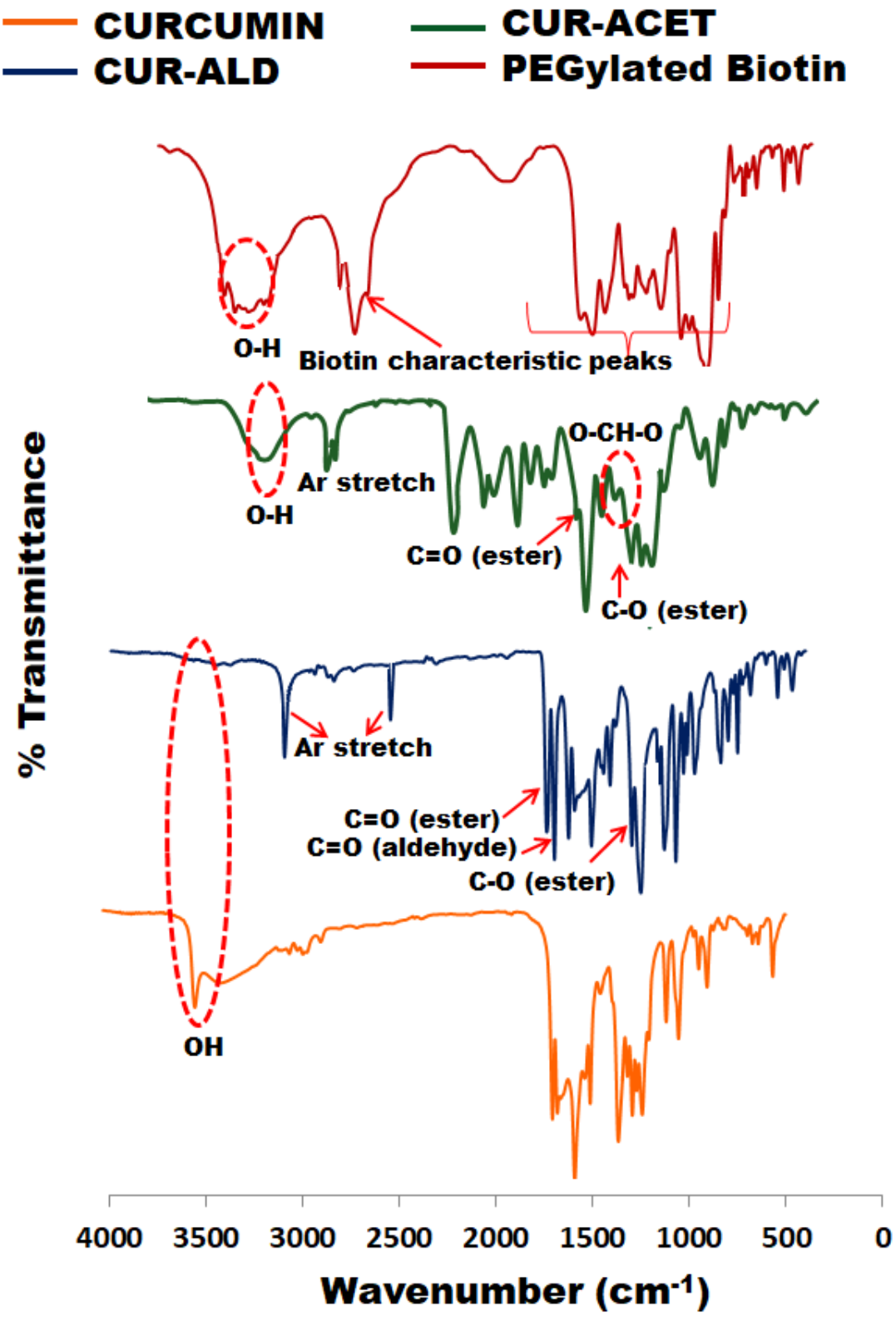

Figure 5.6: FTIR spectra overlay

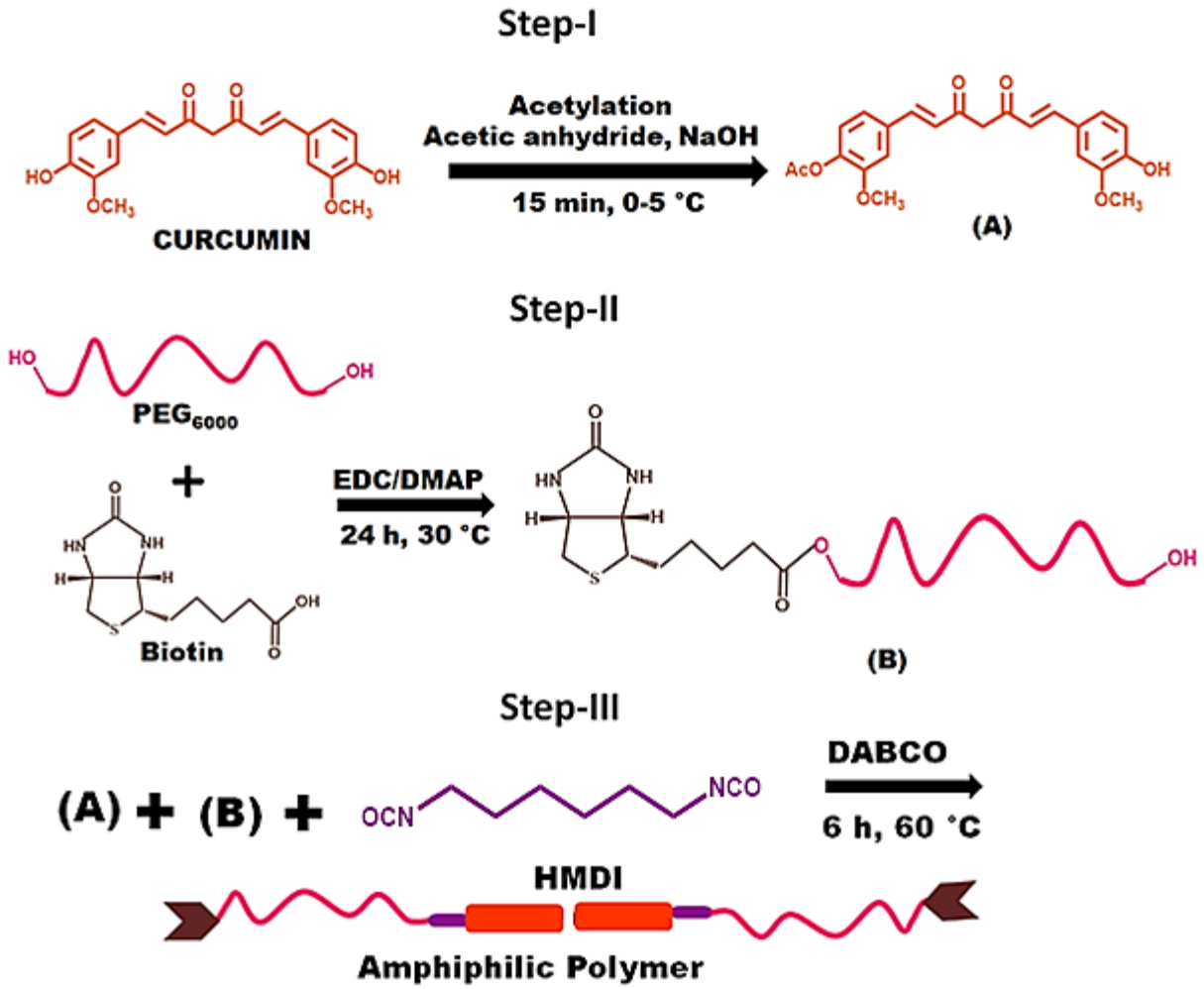

Scheme 5.2: Schematic representation of the synthetic route for preparing biotin tagged curcumin derived amphiphilic polymer devoid of acetal linkage and stimuli response

The Mn values of B-CUR-(A)-P1 to P3 and B-CUR-P4 were determined as mentioned in **table 5.1** by comparing the integrals of signals at δ 7.60 (aromatic proton of curcumin block) and δ 3.51 (methylene protons of PEG block) as well as by GPC measurements **figure 5.7**.

Table 5.1: Characteristics of curcumin polymer prodrug

Prodrug	M_n (^{1}H NMR)	M_n[a] (GPC)	PDI[a]	Curcumin loading[b] (wt %)
	(kg mol^{-1})			
B-CUR-(A)-P1	5.66	-	-	6.5
B-CUR-(A)-P2	5.74	-	-	6.4
B-CUR-(A)-P3	5.83	7.27	1.06	6.3
B-CUR-P4	2.08	6.94	1.1	-

[a]Determined using GPC (eluent used was DMF at a flow rate of 0.75 ml/min using PMMA standards at 40 °C), [b]Calculated as per equation ($MW_{curcumin}/M_{n, NMR}$)

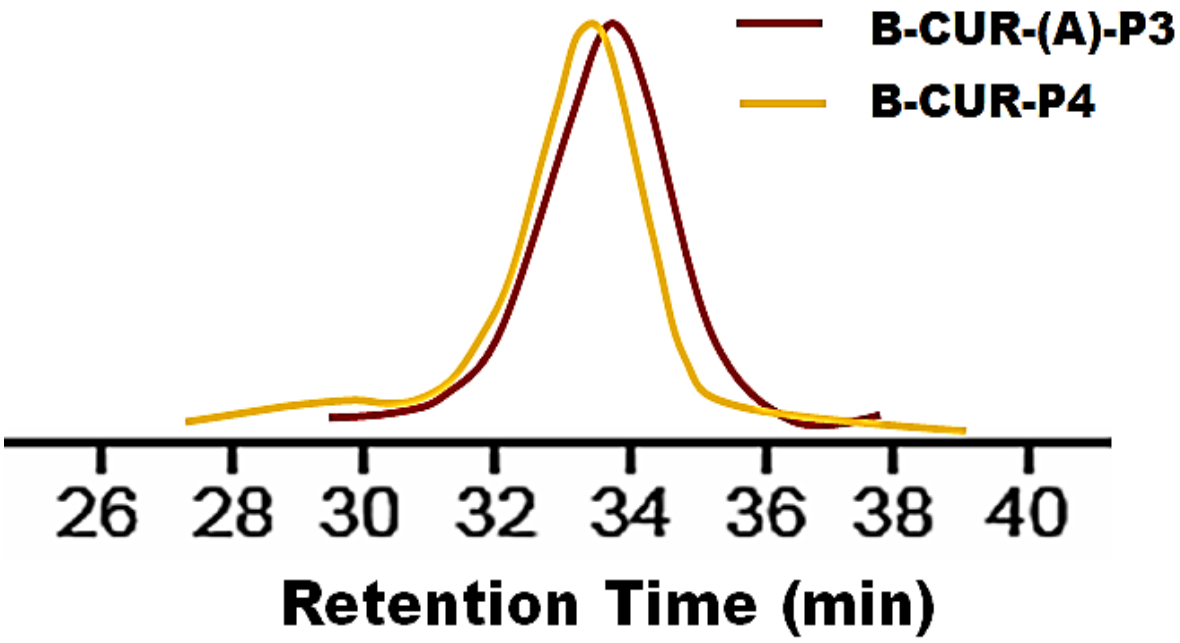

Figure 5.7: GPC curves of the responsive and non-responsive polymers.

5.3.2 Self-assembly of amphiphiles into micelles

The micelles were prepared from the amphiphiles via solvent exchange method. All the 4 micellar systems, i.e. three acetal-ester linkage containing B-CUR-(A)-P1, P2, P3 and one acetal

devoid B-CUR-P4 showed a mono-modal size distribution as evident from DLS studies. The average size of these micelles fall in the range of 150-200 nm, the size is found to increase upon increasing the Mn of linked PEG unit **(Table 5.1, figure 5.8 B)**. The micelle having PEG_{2000} has the smallest size of 153 nm and the system with PEG_{6000} shows largest size of 210 nm. The size of non-stimuli responsive micelle was found to be 195 nm. The HR-TEM imaging also corroborated with the observations of DLS studies demonstrating a homogeneous particle distribution **(figure 5.8).** The slight decrement in the size of HRTEM measurements as compared to the DLS studies can be attributed to the dehydration of the PEG chains in the process of sample preparation for the analysis[20]. The size distribution and HRTEM images of other micelles have been shown in **figure 5.9**.

Table 5.2: Characteristics of the blank and DOX.HCl loaded curcumin prodrug micelles

System	PEG_X used	CMC[a] (mg/L)	Hydrodynamic Radius R_h[b] (nm)		DLE[c] (wt %)	DLC[c] (wt %)
			Blank	DOX loaded		
B-CUR-(A)-P1	PEG_{2000}	0.81	155 ± 2.5	171 ± 3.1	38	9.5
B-CUR-(A)-P2	PEG_{4000}	0.95	183 ± 1.3	195 ± 1.9	47	12.1
B-CUR-(A)-P3	PEG_{6000}	1.09	210 ± 3.8	223 ± 2.7	63	15.8
B-CUR-P4	PEG_{6000}	4.23	195 ± 1.7	217 ± 1.3	61	14.3

[a]Determined by fluorescence spectrophotometer using pyrene probe [b]Determined by DLS at pH 7.4 [c]Determined by UV-vis spectrophotometer.

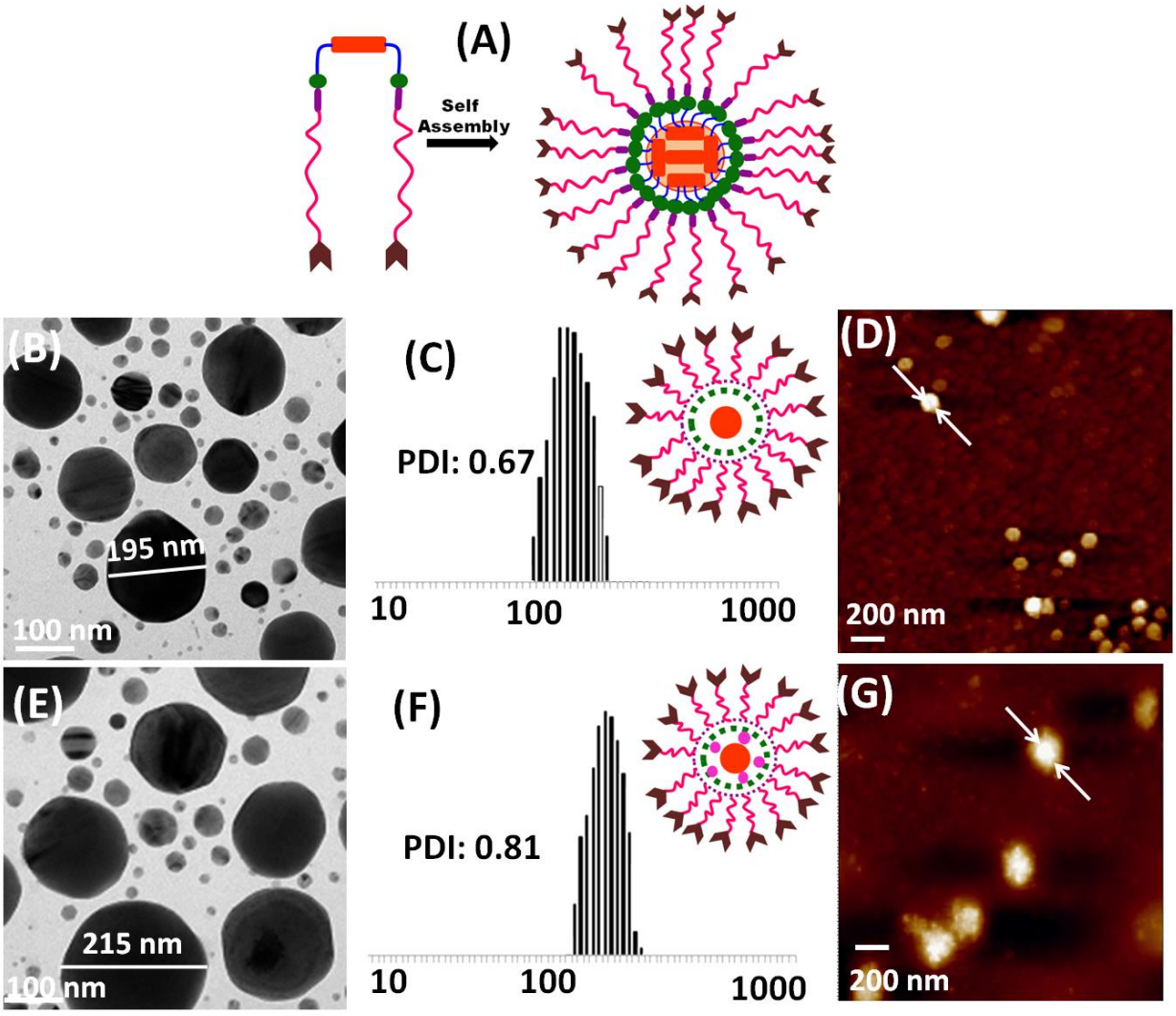

Figure 5.8: (A) Schematic representation depicting self assembly of the amphiphile into curcumin prodrug micelles. Comparison of size and morphology of blank and drug loaded B-CUR-(A)-P3 micelles (B) HR-TEM image (C) size distribution as per DLS spectra (D) AFM image of blank micelle and (E) HR-TEM image (F) size distribution as per DLS spectra (G) AFM image of DOX loaded micelle.

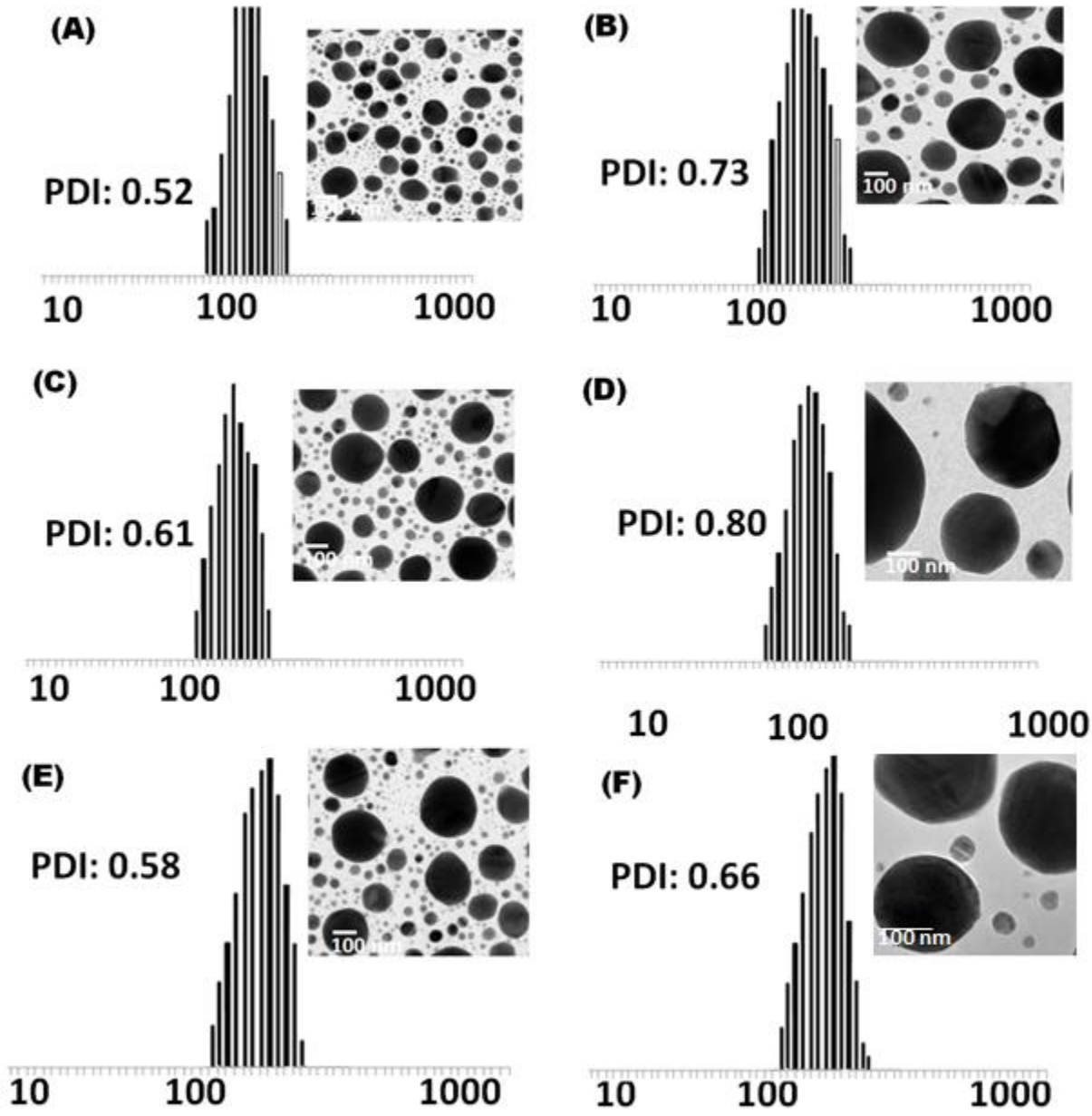

Figure 5.9: Size distribution as observed from DLS histograms and inset HRTEM images of (A) blank B-CUR-(A)-P1, (B) DOX loaded B-CUR-(A)-P1, (C) blank B-CUR-(A)-P2 (D) drug loaded B-CUR-(A)-P2, (E) B-CUR-P4 and (F) drug loaded B-CUR-P4

The CMC values were quantified using pyrene as a fluorescence probe. It was observed that, the stimuli responsive micelles B-CUR-(A)-P1 to B-CUR-(A)-P3 exhibited low values of 0.81−1.09 mg/L **(Table 2, figure 5.10)**, indicating that amphiphiles have the ability to form highly stable micelles.

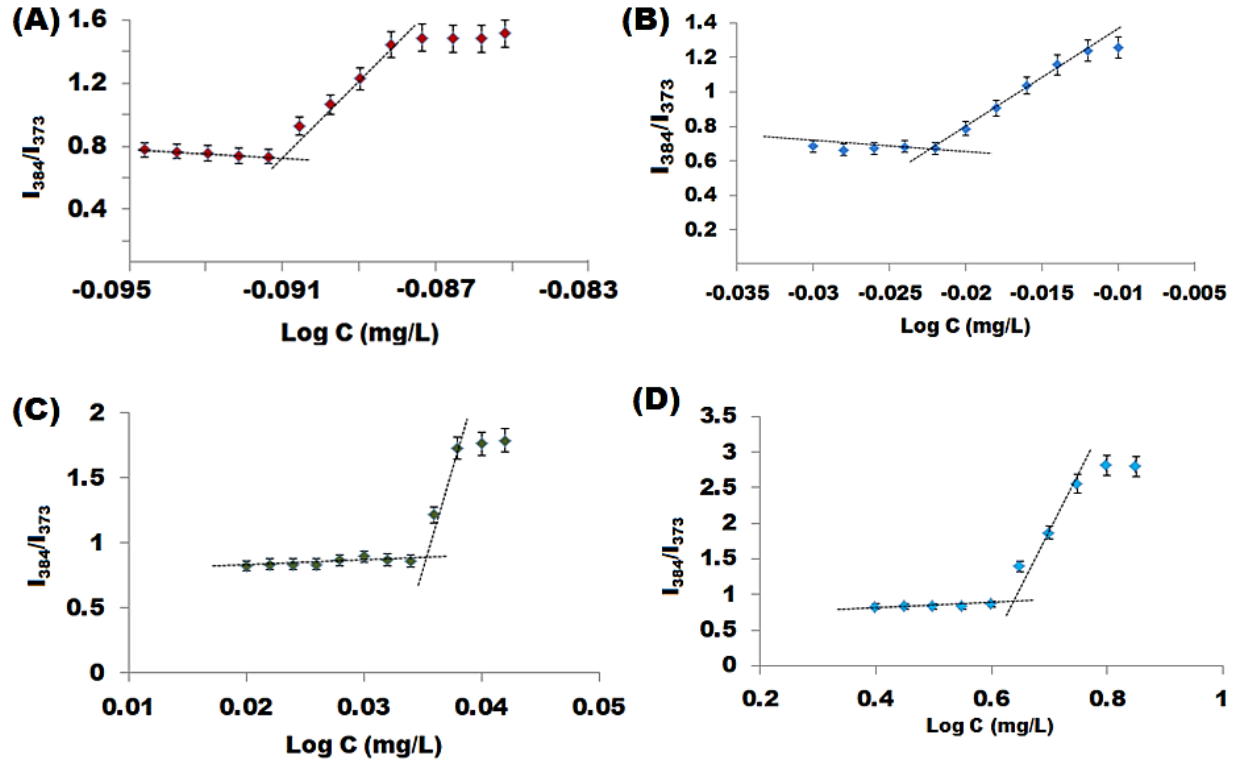

Figure S8: The CMC determination of (A) B-CUR-(A)-P1, (B) B-CUR-(A)-P2, (C) B-CUR-(A)-P3 and (D) B-CUR-4 using pyrene as the fluorescent probe. The data were represented as mean ± standard deviation (n = 3).

On the other hand, B-CUR-P4 exhibits a relatively high CMC value of 4.23 mg/L. This observation is supported by a well-known fact from the literature that states that, the ratio of hydrophobic portion in an amphiphile has an effect on the CMC value[21]. A higher ratio of hydrophobic counterparts results in a smaller CMC value. The higher hydrophobicity of the responsive amphiphiles is attributed to the presence of aromatic rings of p-formyl benzoic acid and methyl groups of TME in the polymer skeleton in addition to the hydrophobicity contribution from curcumin and methyl groups of HMDI. However in the nonresponsive amphiphile, the hydrophobicity comes only due to the presence of HMDI and curcumin making the hydrophobic ratio smaller than the responsive amphiphiles. Thus the CMC value of this micellar system is much greater as compared to the other three micelles. The relatively low CMC values make the micelles as desirable formulation candidates for intravenous administration as

the effect of dilution upon entering the body on the microstructure of these assemblies would be minimal[22].

5.3.3 Hydrolysis of the acetal linkage containing polymers in response to pH variations

The acetal linkage containing micelles i.e. B-CUR-(A)-P1 to B-CUR-(A)-P3 were subjected to hydrolysis under different pH conditions (4.0, 5.0 and 7.4) at 37°C. The hydrolysis was quantified by monitoring the concentration of its product CUR-ALD at 430 nm by UV-vis spectroscopic determination. The observations of the study showed a dependence of hydrolysis rate on pH of the media. The acetal groups in B-CUR-(A)-P3 micelles showed a 99.2%, 73.6%, and 6.3% degradation at pH 4.0, 5.0 and 7.4, respectively by 10 hours **(Figure 5.10A)**. The half-lives of acetal polymer was found to be 2.8 h at pH 4.0 and 4.9 h at pH 5.0; whereas at pH 7.4, less than 15% acetal hydrolysis occurred even after 24 h. When B-CUR-P4 was subjected to hydrolysis under similar conditions, no polymeric degradation was observed confirming that the presence of a labile acetal linkage is imperative for pH responsive hydrolysis[23].

The change in size of micelles as a response to the acidic hydrolysis was also determined by DLS measurements. As there is hardly any degradation at pH 7.4, there is a minimal change in the size of the micelles even after 24 h **(figure 5.10B)**. On the contrary, the micelles subjected to conditions of pH 5.0 showed a drastic size variation. There is a fast swelling of the polymer chains initially that is evident from the increase in size of the micelles from 210 nm to 345 nm in the first 2 hours. At about 12 h the size increased to more than 750 nm. After 24 h of incubation when complete degradation is expected, small sized unimers of size less than 10 nm were observed which suggests complete dissolution of the polymer following complete hydrolysis. These size changes are more rapid at time intervals of 2 h and 12 h when the polymers are subjected to pH 4.0 which as result of the shorter half-life of the acetal linkage at pH 4.0. The non-responsive micelles however did not show any variation in size that is evident from **figure 5.10 C.**

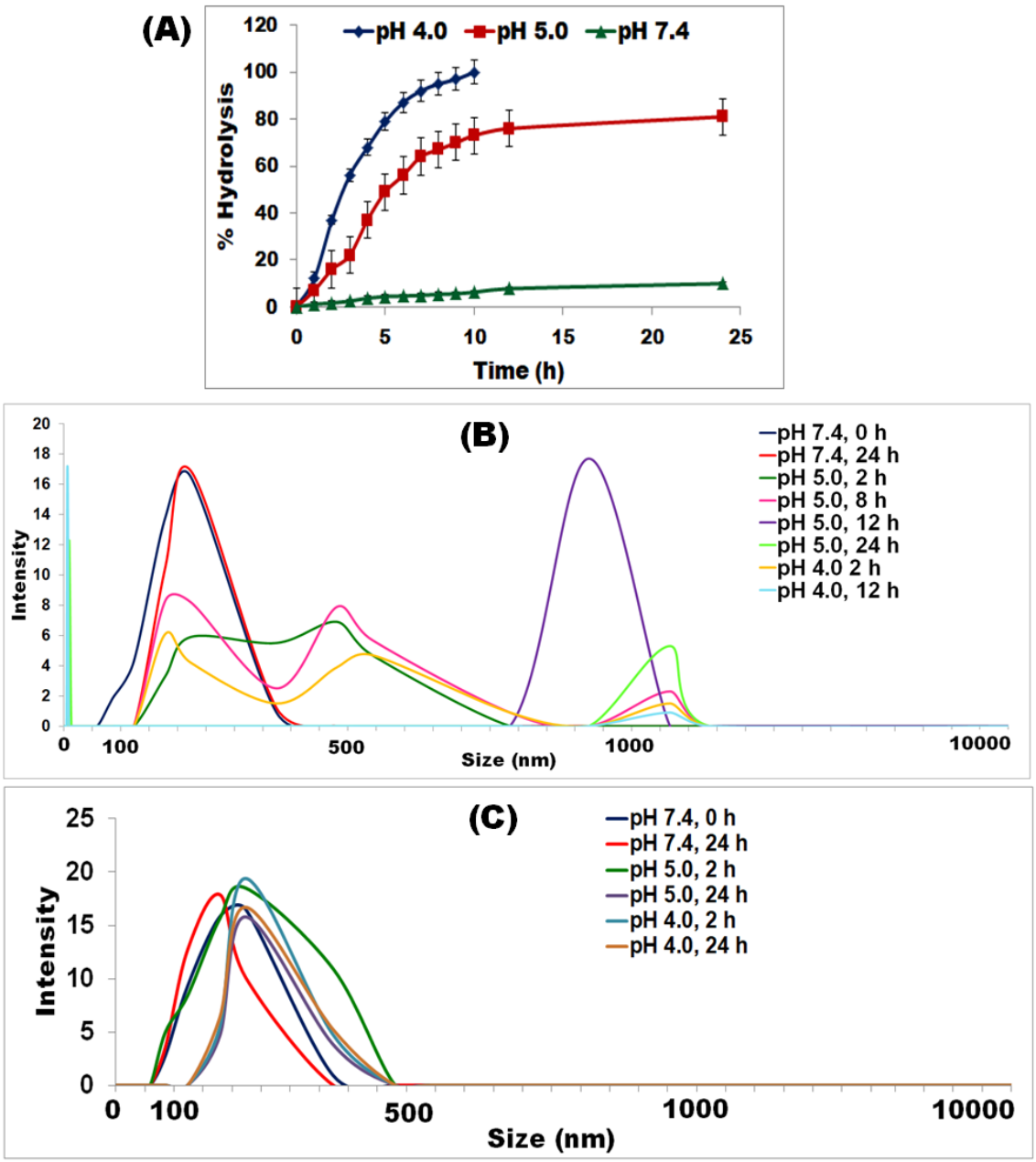

Figure 5.10: (A) Acidic hydrolysis of acetal linkage containing B-CUR-(A)-P3 polymer. DLS histograms representing changes in size distribution of DOX loaded (B) B-CUR-(A)-P3 micelles and (C) B-CUR-P4 micelles under various pH conditions at 37 °C at different time intervals upon exposure to hydrolytic conditions.

5.3.4 Loading and in Vitro Release of DOX in response to pH and enzyme

For the assessment of drug entrapment and release behavior of the synthesized micelles, DOX was used as a model hydrophobic drug. The results showed that the acetal linkage containing micelles (i.e. B-CUR-(A)-P1 to B-CUR-(A)-P3 demonstrated loading capacities in the range of 9.5−15.8 wt%, corresponding to entrapment efficiencies of 38−63 % **(Table 5.2)**. It was observed that loading capacities increased with increasing length of PEG block, most probably due to an availability of more spatial area in bigger cavities of large sized aggregates[24]. The nonresponsive micelle, B-CUR-(A)-P4 demonstrated a DLC of 14.3% and DLE of 61% which are similar to the efficiency of B-CUR-(A)-P3. The loading of DOX resulted in ~20 nm increase in the micelle size for all the micellar carriers. Further, the amount of curcumin content was quantified using ^{1}H NMR and the loading % was found to be in the range of 6.0-6.5 wt% as shown in **table 5.1**.

Figure 5.11A and **5.12A** gives a schematic representation of the phenomenon of drug release from the responsive micelles.

The in vitro release studies were executed at 37 °C by subjecting to various pH values (i.e. 4.0, 5.0 and 7.4). B-CUR-(A)-P1, B-CUR-(A)-P2 and B-CUR-(A)-P3 these three micelles demonstrated a reasonably rapid release of DOX upon exposure to acidic conditions as compared to the physiological pH 7.4 **(Figure 5.11 B, C & D)**. For example, B-CUR-(A)-P3 demonstrated ~97% and 75% of DOX release within 30 h at pH 4.0 and 5.0, respectively. Whereas, <30% of drug was observed at pH 7.4 at other similar conditions. The drug release rate was found to exhibit a minimal increase at the same pH value upon with increased PEG molecular weights. However in the nonresponsive polymer there is no effect in the release rate upon change of pH of release media as expected. It was observed that, less than 40% of DOX could be released under all three pH conditions even after a substantial time interval of 48h **(figure 5.11 E)**. This is attributed to the inability of nonresponsive polymer to undergo major structural changes with variation of pH due to the absence of acid labile units in its structure. The negligible DOX release occurs simply by escape of DOX molecules from the polymer upon its minimal swelling in release media. This type of release is undesirable as there are chances of drug leakage during circulation prior to reaching the target tissues. These results provide evidence that, presence of functionalities that are responsive to tumor milieu play a significant role in avoiding leakage of

drug from the carrier[25,26]. This is also crucial to avoid induction of toxic effects on healthy cells if drug leakage occurs from the carrier en-route.

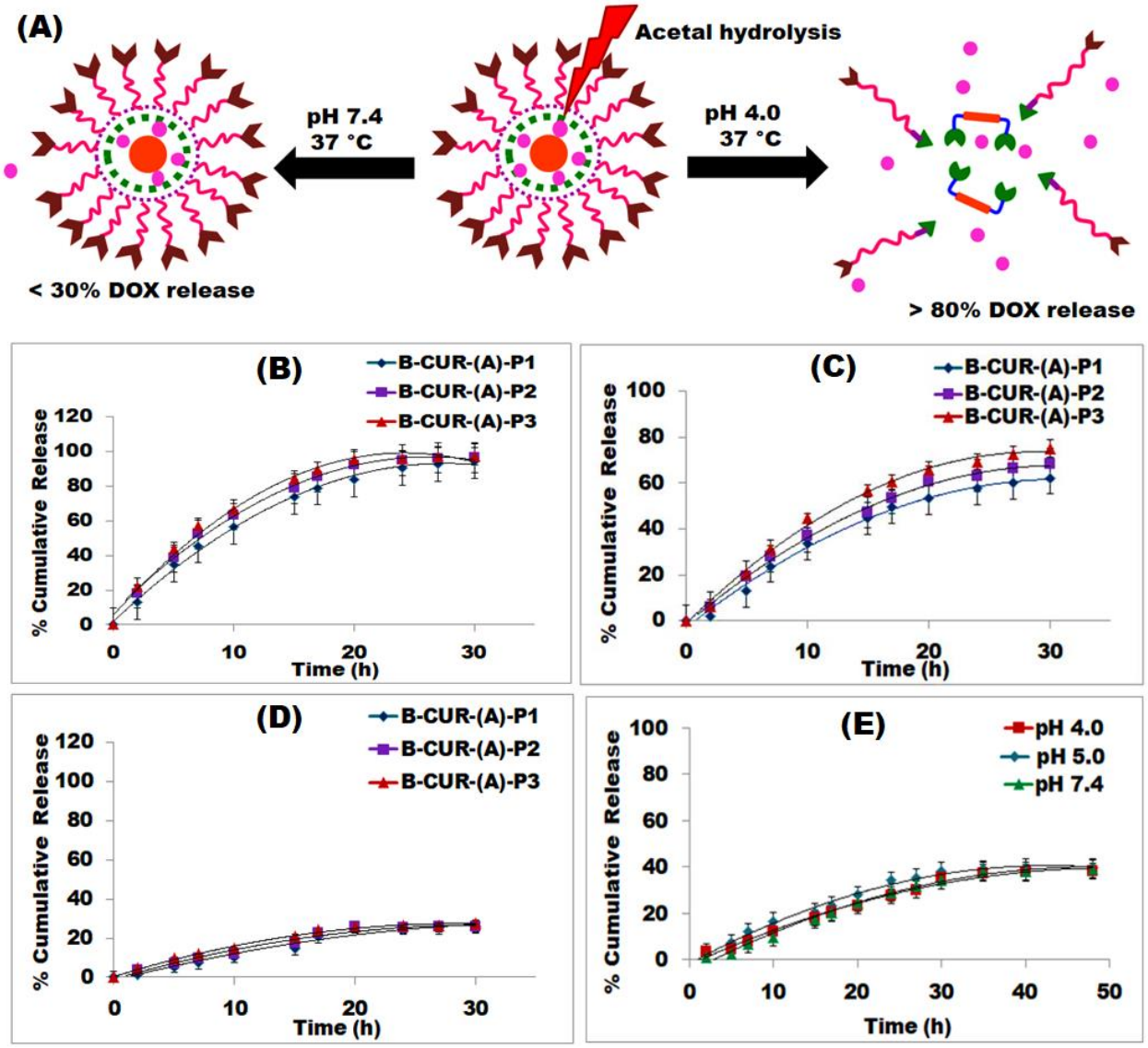

Figure 5.11: (A) Schematic representation of DOX release from micelles upon acetal hydrolysis at pH 4.0, 37°C. Percent cumulative release profile of DOX from acetal linkage containing polymers at pH (B) 4.0 (C) 5.0 and (D) 7.4. (E) The comparison of DOX release from non-responsive polymer under all three pH media.

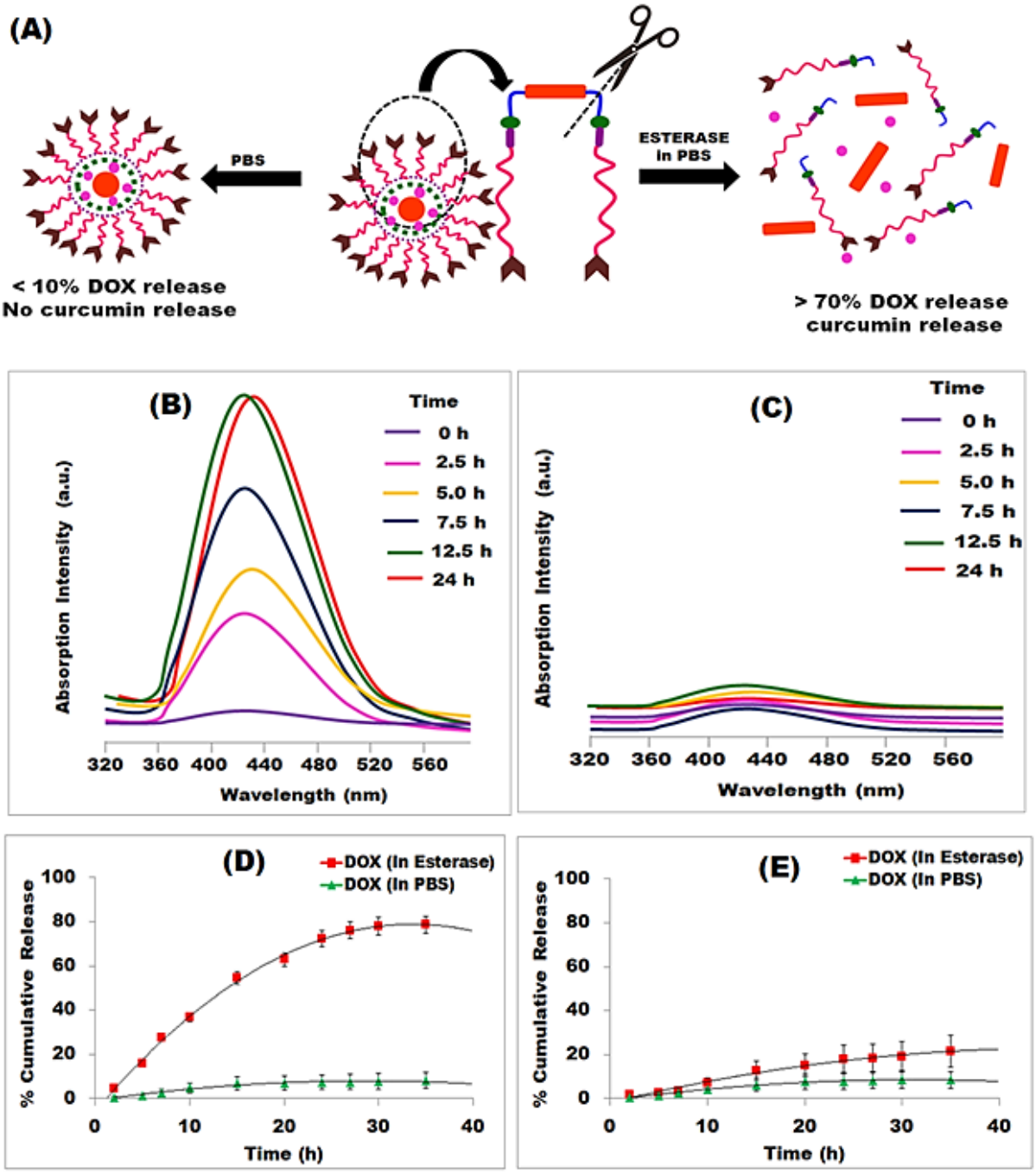

Figure 5.12: (A) Schematic representation of DOX and curcumin release from micelles under the influence of esterase enzyme in PBS at 37°C. UV-vis spectra showing release/no release of curcumin from B-CUR-(A)-P3 in (B) presence and (C) absence of esterase at different time intervals. Percent cumulative release of DOX from (D) responsive micelle B-CUR-(A)-P3 & (E) non-responsive micelle.

The prodrug curcumin upon release post acetal hydrolysis was designed to attain its active drug form by cleavage of ester bond by enzymatic degradation. This was assessed by subjecting B-CUR-(A)-P3 to 5U of esterase enzyme and the release of curcumin was monitored by UV-vis spectrophotometric determinations. The UV-vis spectra demonstrated, increase in intensity of curcumin in the release media with increasing time interval **(figure 5.12B)**. On the contrary no curcumin was detected in the release media in absence of esterase even after 24 h **(figure 5.12C)**. However the non-responsive micelle did not show the presence of curcumin in the release media. The cumulative percent release graphs as shown in **figure 5.13** showed >60% of curcumin release in presence of esterase and <10 % in only PBS.

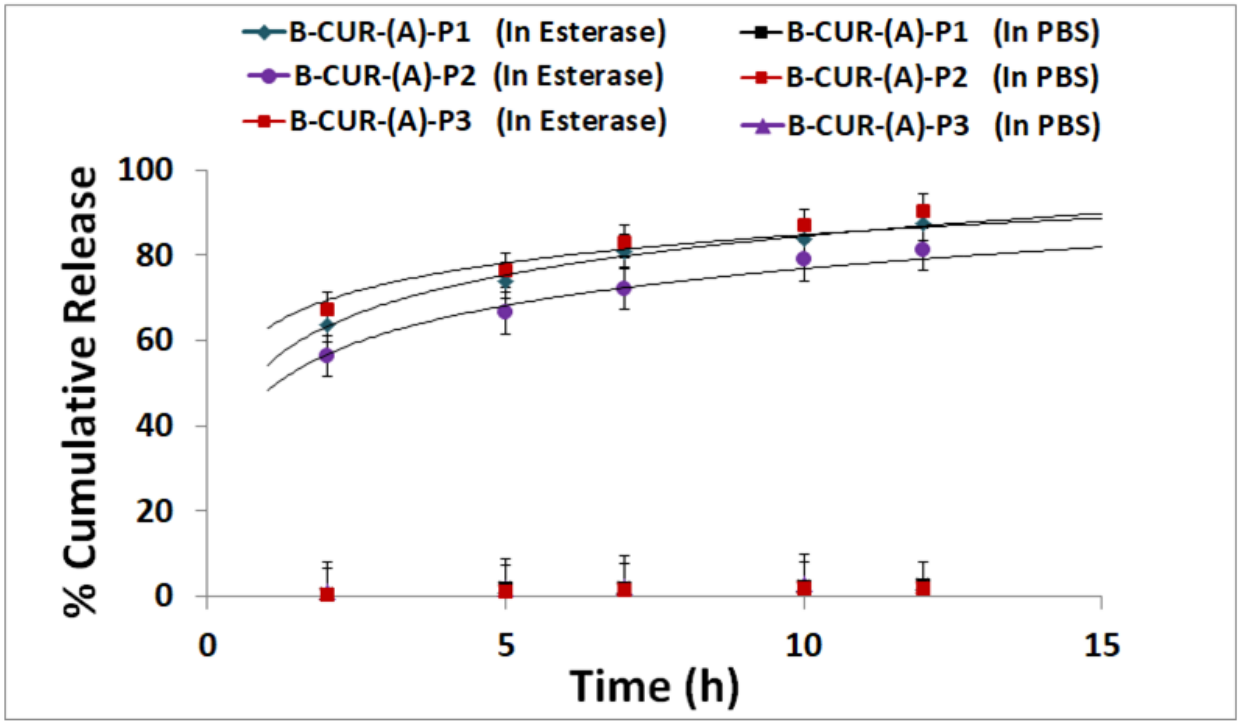

Figure 5.13: Percent cumulative release of curcumin from micelles in presence and absence of esterase at 37°C.

The enzymatic trigger causing the removal of curcumin with its pro-moiety causes the micelle to disassemble due to loss of hydrophilic and hydrophobic balance that causes the entrapped DOX molecules to be released as well. This is evident from the UV-vis spectrophotometric determinations carried out at the excitation wavelength of DOX i.e. 480 nm. **Figure 5.12D** depicts the percent cumulative release of DOX in the presence and absence of esterase.

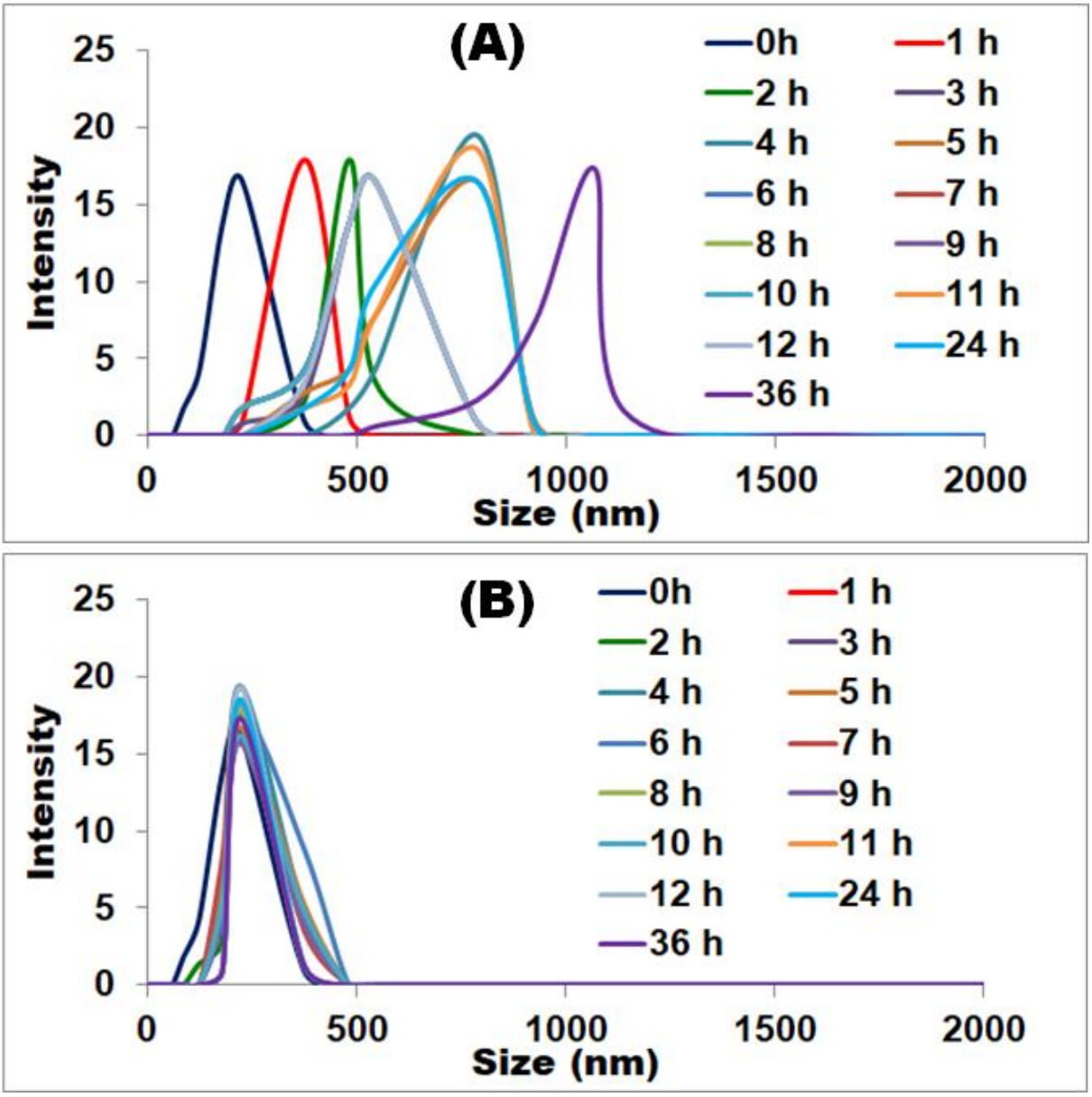

Figure 5.14: DLS histograms representing size distribution of DOX loaded (A) B-CUR-(A)-P3 micelles and (B) B-CUR-P4 micelles in the presence of esterase in PBS at 37 °C at various time intervals.

When PBS solution of pH 7.4 is the release media, <10% of DOX molecules were detected and upon exposure to esterase, >70% of DOX molecules are released. The % cumulative release of DOX on the other hand from nonresponsive micelles is less than 20 % even when esterase is

present as depicted in **figure 5.12E**. The changes in size of the micelles were also followed by DLS measurements **(figure 5.14A)**. DOX loaded B-CUR-(A)-P3 micelles upon enzymatic degradation showed increase in the size from 225 nm at 0 h to > 500 nm at 24 h. After micellar disassembly, the polymer fragments generated tend to agglomerate and form large polymer aggregate. This phenomenon explains the observation of increase in size. The DOX loaded non-responsive micelles do not show any change in size **(figure 5.14B).**

The stability of DOX loaded micelle in blood plasma was also determined. The changes in size of the drug loaded carriers were determined via DLS measurements (as shown in **figure 5.15**).

The size of the micelles in FBS was close to those formed in PBS. It is evident from the graph that the micelles are stable even after 24 hours. This study is corroborated by following the release of DOX and curcumin from B-CUR-(A)-P3 after incubation in FBS at 37 °C.

The release was analyzed via UV-vis spectrophotometric determination **(figure 5.16)**. The DOX loaded curcumin containing micelle was found to be stable with <20% release of both DOX as well as curcumin. This study confirmed the stability of the synthesized carrier even in the presence of proteins. The micelles had the capability of preserving >70% of drugs. Thus indicating that, the micelles can undergo cleavage only upon their exposure to esterase present in intracellular lysosomes.

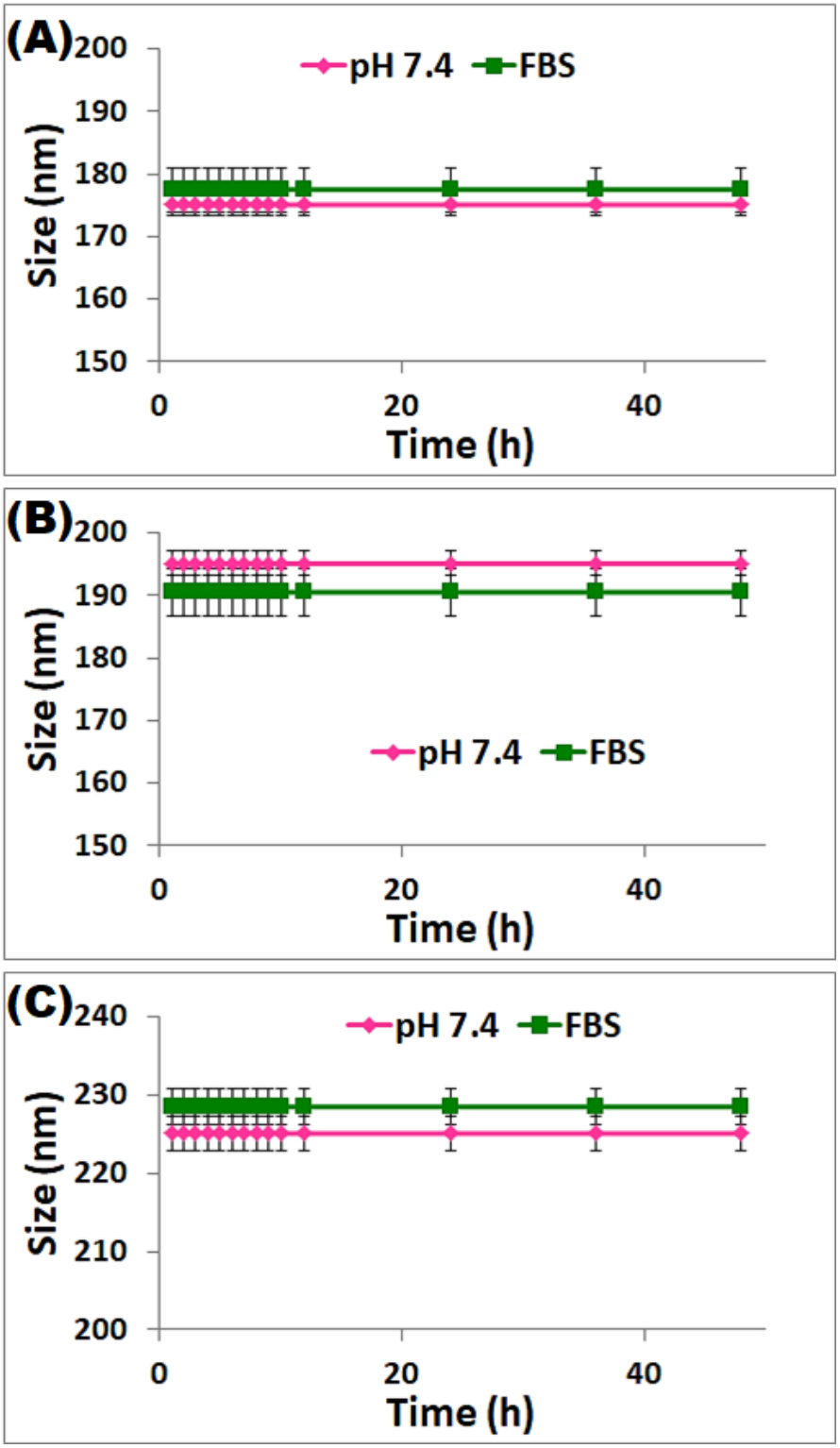

Figure 5.15: Comparison of size vs. time plots for demonstrating the stability of DOX loaded micellar carriers (A) B-CUR-(A)-P1 (B) B-CUR-(A)-P2 and (C) B-CUR-(A)-P3 in PBS (7.4) and FBS at various time intervals

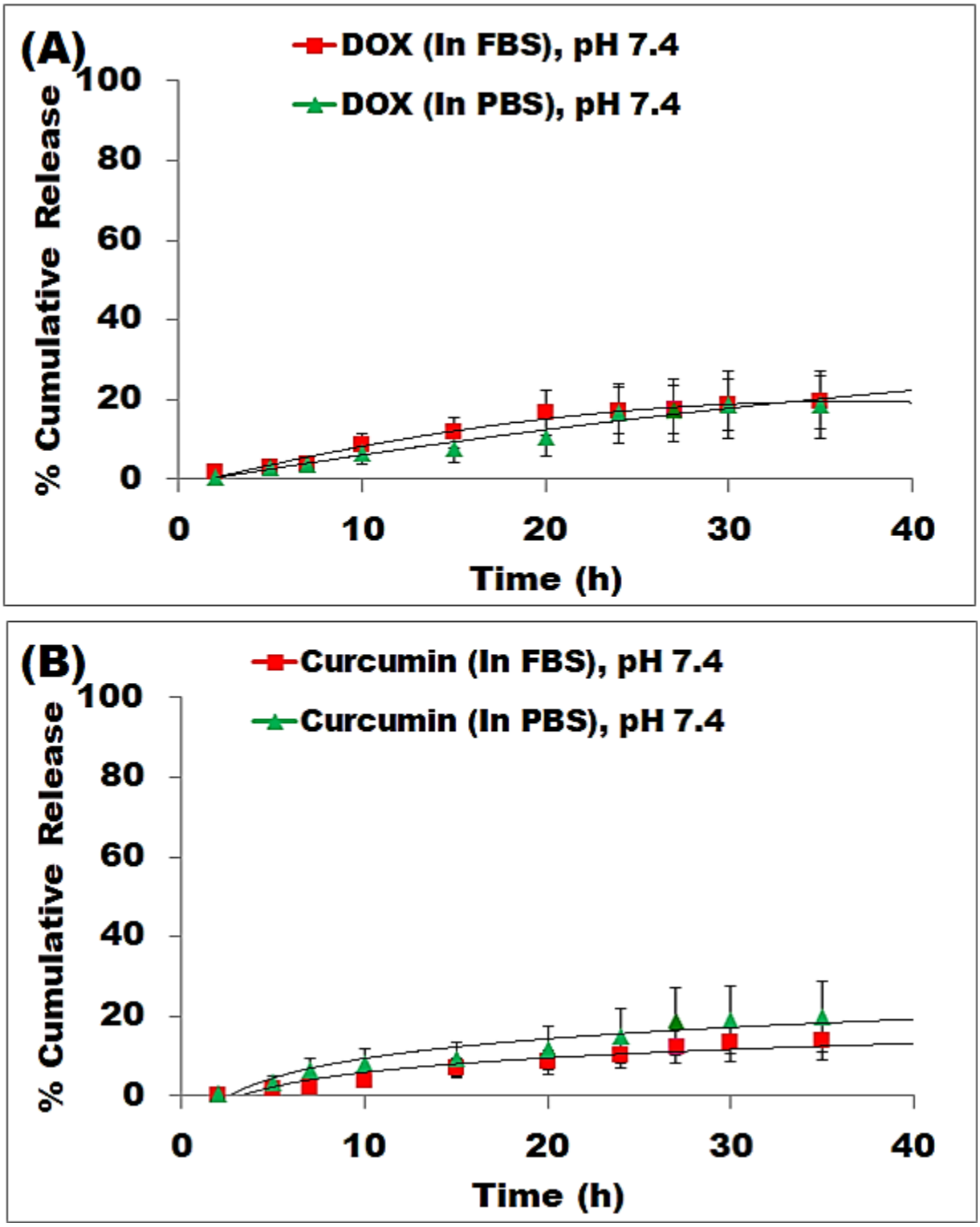

Figure 5.16: Comparison of the percent cumulative release profiles of (A) DOX and (B) curcumin from B-CUR-(A)-P3 in PBS and FBS at pH 7.4 at 37°C.

5.3.5 Targeting ability and antitumor activity of DOX loaded targeting micelles and a comparison of responsive disassembling micelles with non-responsive one

The first step involved evaluation of the cytotoxicity of the blank micelles, to ascertain their suitability as drug carriers. The in-vitro cytotoxicity of B-CUR-(A)-P1 to B-CUR-(A)-P3 and B-CUR-P4 was tested on HepG2 (liver cancer cell line) as well as on non-cancerous NIH-3T3 fibroblasts using MTT assay **(figure 5.17 A & B)**. The results shown in figure suggest no toxicity on both cancer as well as normal cell line suggesting its compatibility to act as drug carriers.

Further, the assessments of the micelles to act as drug carriers was performed using DOX-loaded micelles as well as free DOX and curcumin on HepG2 cell lines. As demonstrated in **Figure 5.17 C** the cell viability post incubation with free DOX and DOX-loaded B-CUR-(A)-P1, B-CUR-(A)-P2, B-CUR-(A)-P3 and B-CUR-P4 for 24 h at different concentrations. The results suggested maximum toxicity of DOX-loaded B-CUR-(A)-P3 with a cell viability of less than 30% at 2.5 µg/ml of DOX concentration. On the other hand, B-CUR-P4 did not induce impressive cell toxicity as ~70% of cells were viable at 2.5 µg/ml of DOX concentration.
As shown in **figure 5.17 D** when the cells dosed with B-CUR-(A)-P3 were treated with esterase, the micelles are able to induce an anticancer effect by killing >60% of the cells at 5 µg/ml of curcumin concentration.

Since the carriers are conjugated with biotin receptor, the targeting ability of the carriers was also evaluated via MTT assay. The cytotoxicity observed on biotin receptor positive HepG2 cell lines was compared with NIH/3T3 fibroblasts that are biotin receptor negative. There is an enhanced cytotoxicity of DOX loaded micelles on HepG2 (~80%) as compared to fibroblasts (<10%). This occurs primarily because no specific interactions exist between NIH/3T3 and biotin leading to an inefficient internalization of the carriers thus exerting no cytotoxicity to normal cell.

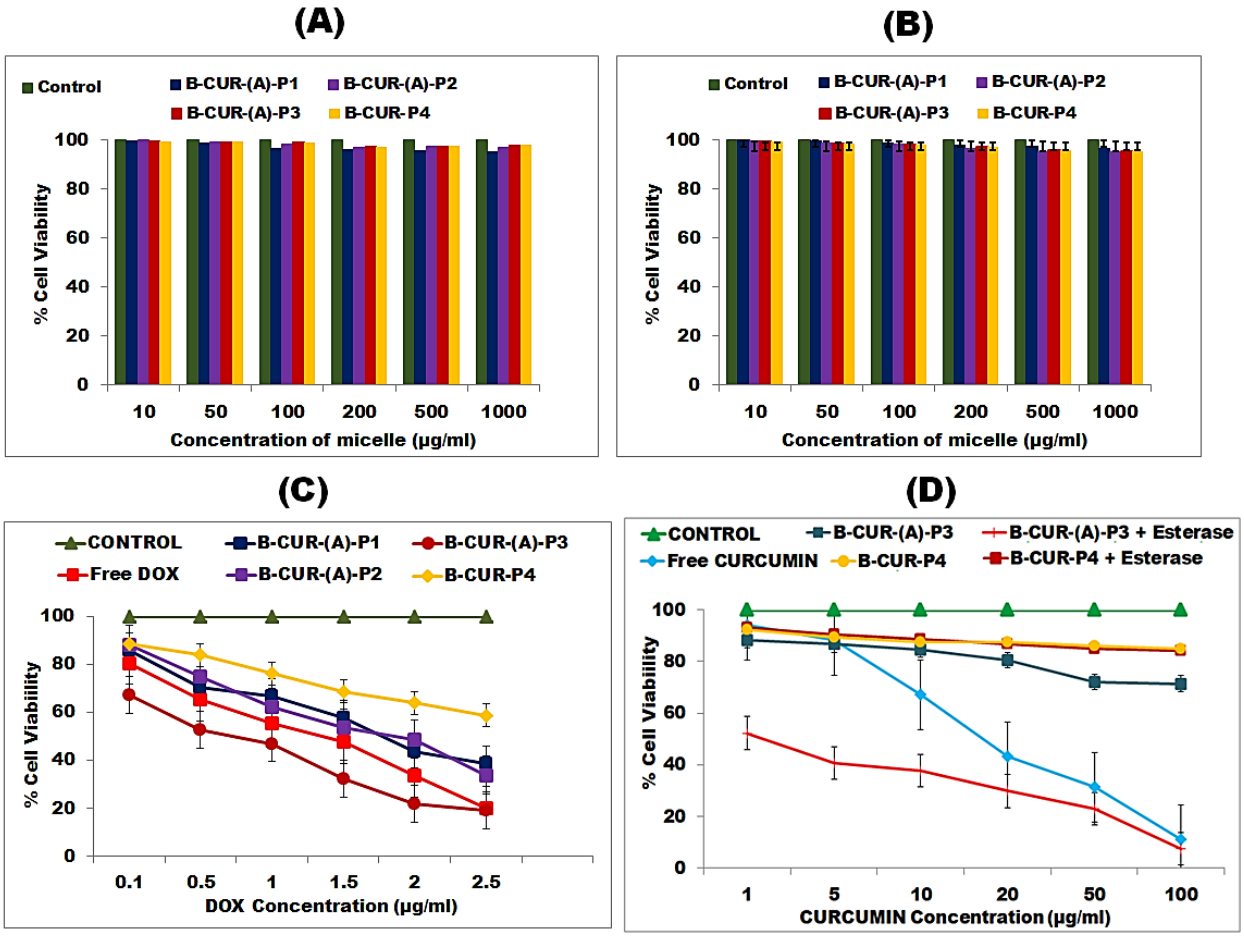

Figure 5.17: Non-toxicity of the carriers as observed by MTT assay on (A) NIH/3T3 fibroblasts and (B) HepG2 cell lines. In vitro cytotoxicity of (C) free DOX and DOX loaded micelles on HepG2 cells post 24 h of incubation. (D) Comparison of in-vitro cytotoxicity of free curcumin, enzyme responsive B-CUR-(A)-P3 and non-responsive B-CUR-P4 micelle on HepG2 cells pretreated with/without 5 U esterase enzyme after 24 h of incubation.

To further confirm receptor specificity mediated internalization of carriers and subsequent cell death, the MTT assay was carried out using DOX loaded micelles in the presence of 1 mg/ml of free biotin (as shown in **figure 5.18**). As expected, there was a retarded cell death because the free biotin molecules blocked the receptors and hindered the internalization of the DOX loaded micelles[27]. While the DOX-loaded **B-CUR-(A)-P3** demonstrated more than 80% cell death at 2.5 µg/ml of DOX concentration, the biotin pretreated cell lines were capable of causing only ~60% cell death at the same concentration. This study is thus a corroborative evidence that, death of

HepG2 cells occurred via an enhanced cellular uptake promoted by biotin. These results confirmed that employing target molecules can improve efficiency of drug delivery to cancer cells.

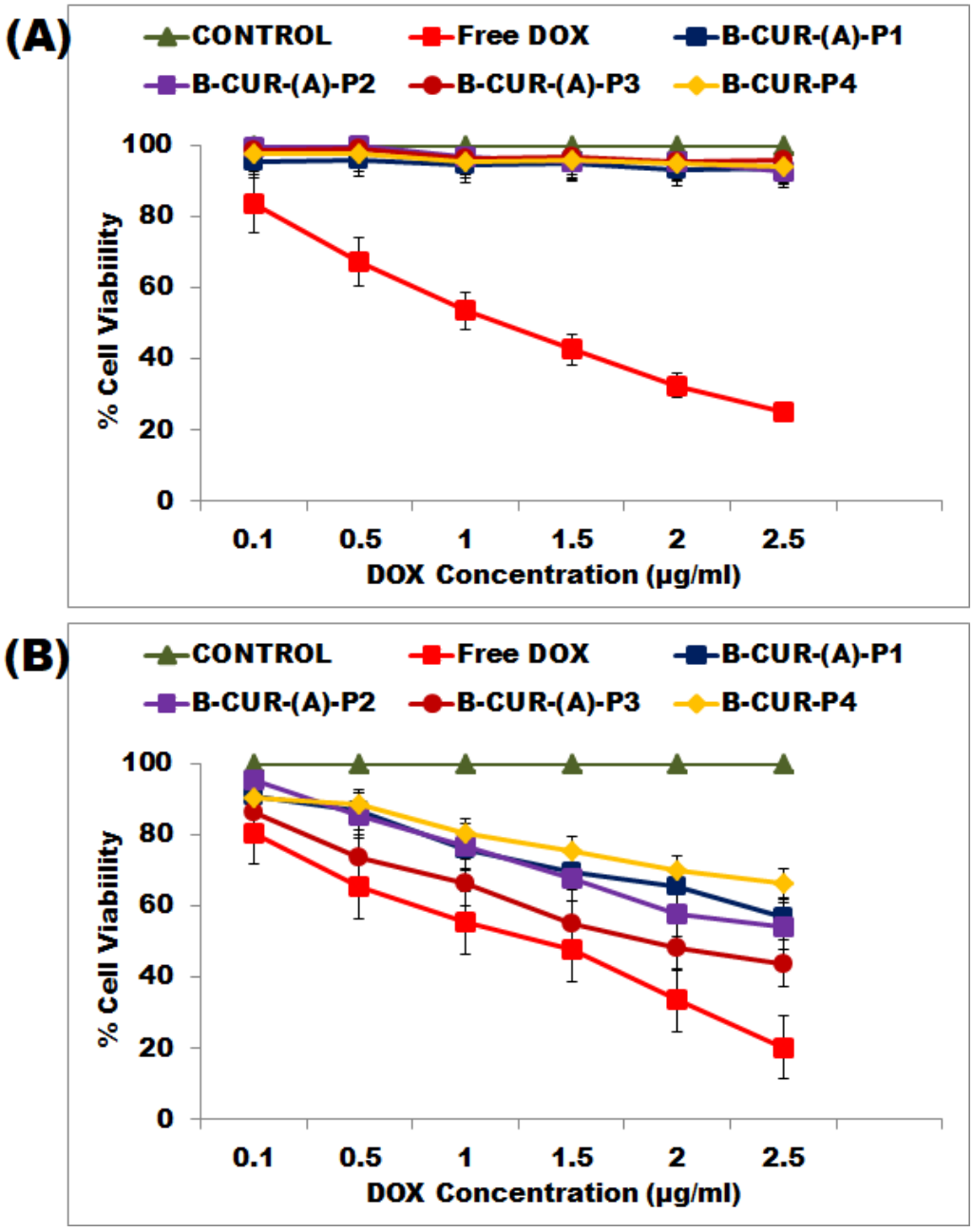

Figure 5.18: (A) MTT assay of DOX loaded micelles on normal NIH3T3 fibroblasts (B) MTT assay of DOX loaded micelles on cancerous HEPG2 cell lines pretreated with 1 mg/ml of biotin.

5.3.6 Combination Index Analysis:

Since the carriers are expected to release 2 drugs in the tumor microenvironment, the performance of the drug pair (curcumin and DOX) for cocktail chemotherapy was evaluated by MTT assay on HEPG2 cell lines **(figure 5.19)**. The combination effect was quantified by calculating the combination index (CI)[28] as per **equation (4)**:

$$\mathbf{CI}_{CCT} = \left[\frac{IC_{50}(Combination\ DOX)}{IC_{50}(DOX)}\right] + \left[\frac{IC_{50}(Combination\ CUR)}{IC_{50}(CUR)}\right] \quad \text{-------- (4)}$$

Here,

CI_{CCT} represents the combination index of cocktail chemotherapy, IC_{50} (combination DOX) and IC_{50} (combination CUR) represents the half inhibitory concentration of DOX and curcumin when used in combination. IC_{50} (DOX) and IC_{50} (CUR) represent the half inhibitory concentration of the single drug used to attain the similar effect. In the case when CI <1, the drug pair exhibits a synergistic effect, when CI=1 the drug pair works in a combination and when CI>1 it demonstrates an antagonistic behaviour respectively.

The calculated values of CI for **B-CUR-(A)-P3** is shown in **Table 5.3**. The IC50 values of both the drugs were found to decrease upon conjugation in the micellar system. Moreover the obtained CI value was less than 1 suggesting that the drug pair induces a synergistic effect in the treatment.

Table 5.3: Combination Index for the paired dual drug treatment using B-CUR-(A)-P3

Cell Line	IC_{50} (DOX) (µg/ml)	IC_{50} (CUR) (µg/ml)	IC_{50} (Combination DOX+CUR) (µg/ml)	CI_{CCT}
HepG2	3.53	5.82	0.6132	**0.28**

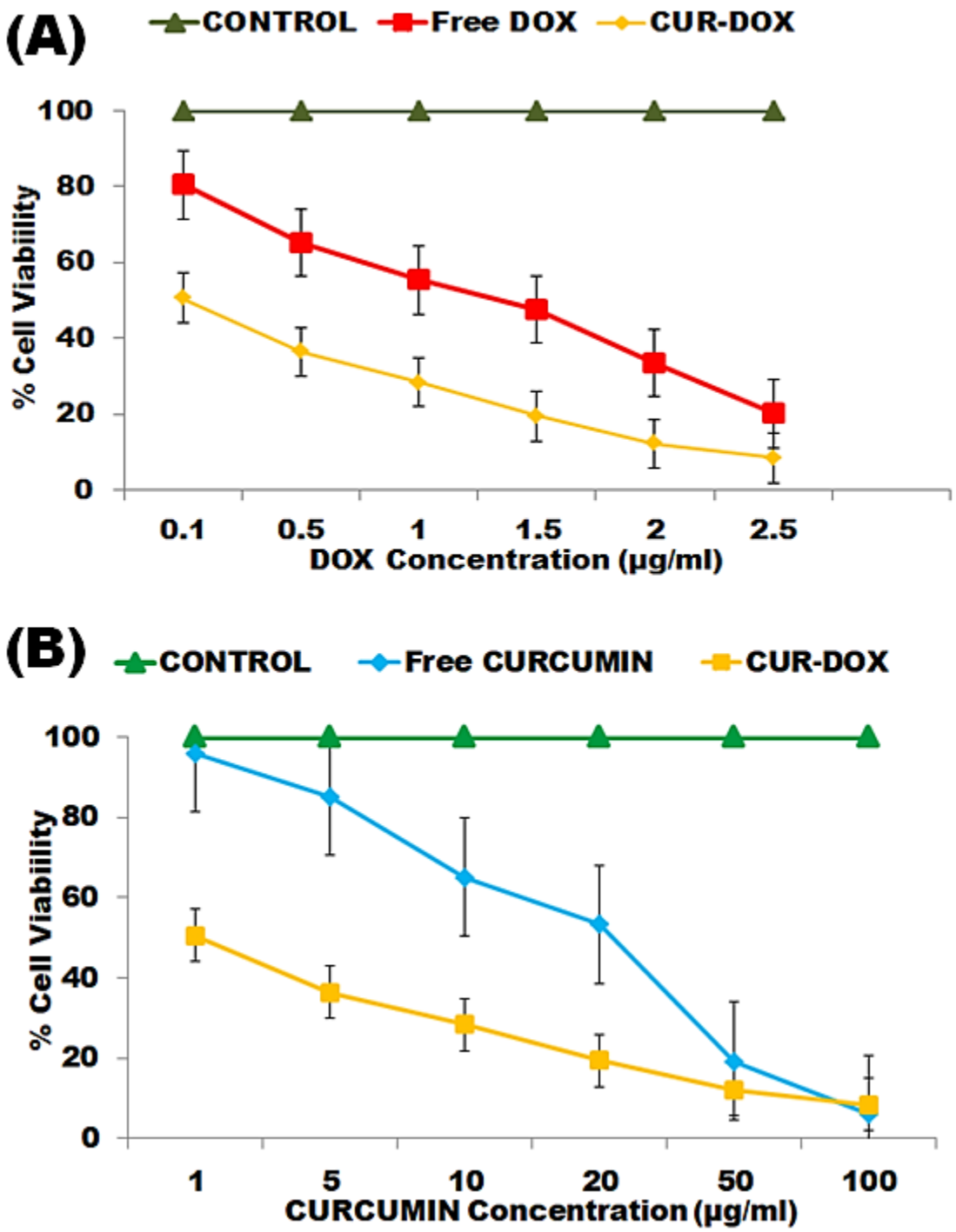

Figure 5.19: Cytotoxicity studies on HepG2 cell lines for calculation of combination index

The cellular internalization of micelles was studied on both HepG2 and NIH/3T3 using fluorescence microscopy. For visualization of the micelles, they were loaded with fluorescein.

The cellular internalization of micelles was studied on both HepG2 and NIH/3T3 using fluorescence microscopy. For visualization of the micelles, they were loaded with fluorescein.

The fluorescence micrographs showed uniformly distributed fluorescence emanating from the fluorescein encapsulated micelles (B-CUR-(A)-P3 and B-CUR-P4) throughout whole cells post 4 h of incubation **(figure 5.20A).** This indicates rapid micellar uptake of HepG2 cells by receptor mediated endocytosis. On the contrary, the biotin tagged micelles could not internalize in the NIH/3T3 cells even after 48 h of dosing as shown in **figure 5.21**.

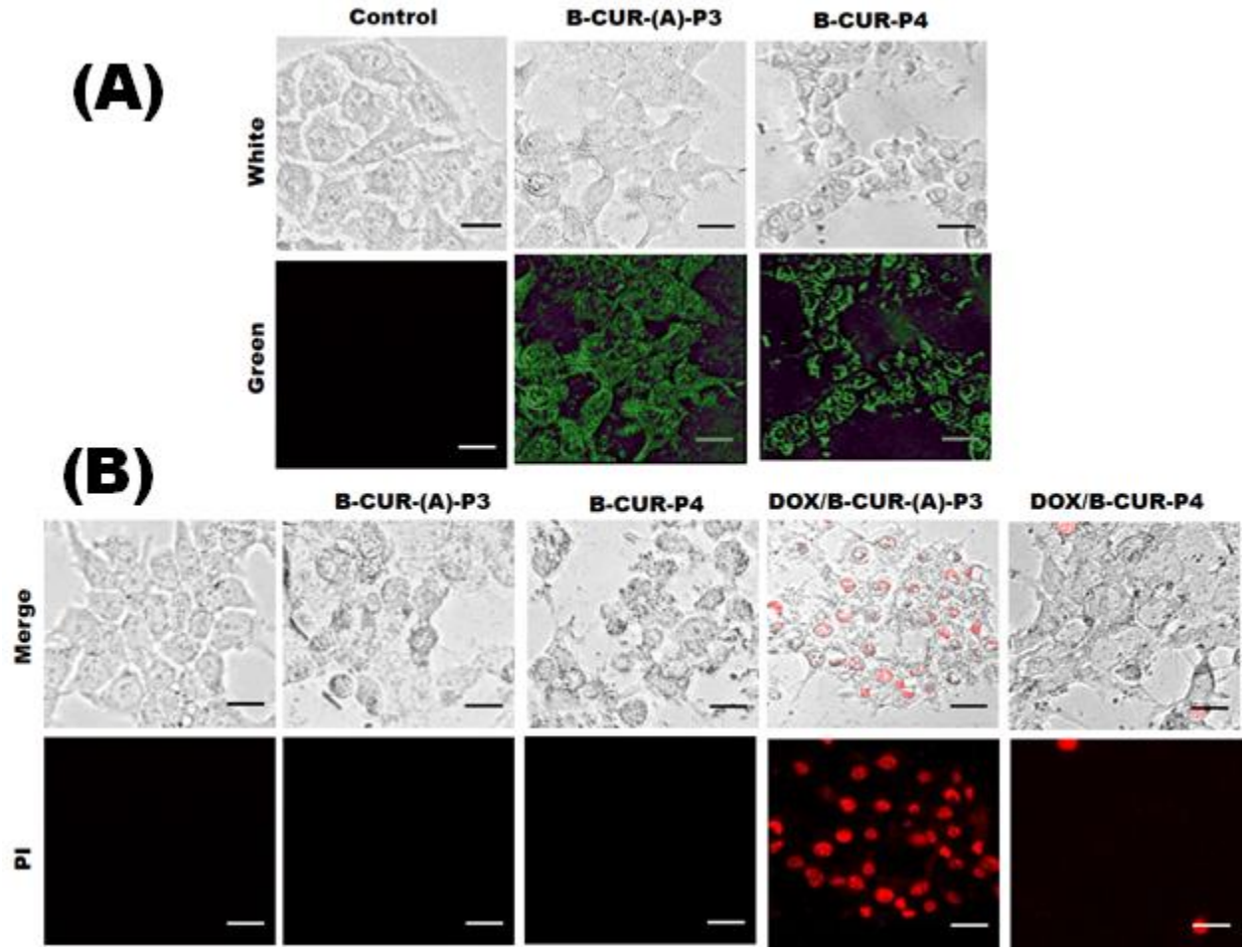

Figure 5.20: Comparison of (A) cellular internalization and (B) Cell viability by PI staining technique of responsive B-CUR-(A)-P3 and non-responsive B-CUR-P4 (Scale- 10 µm)

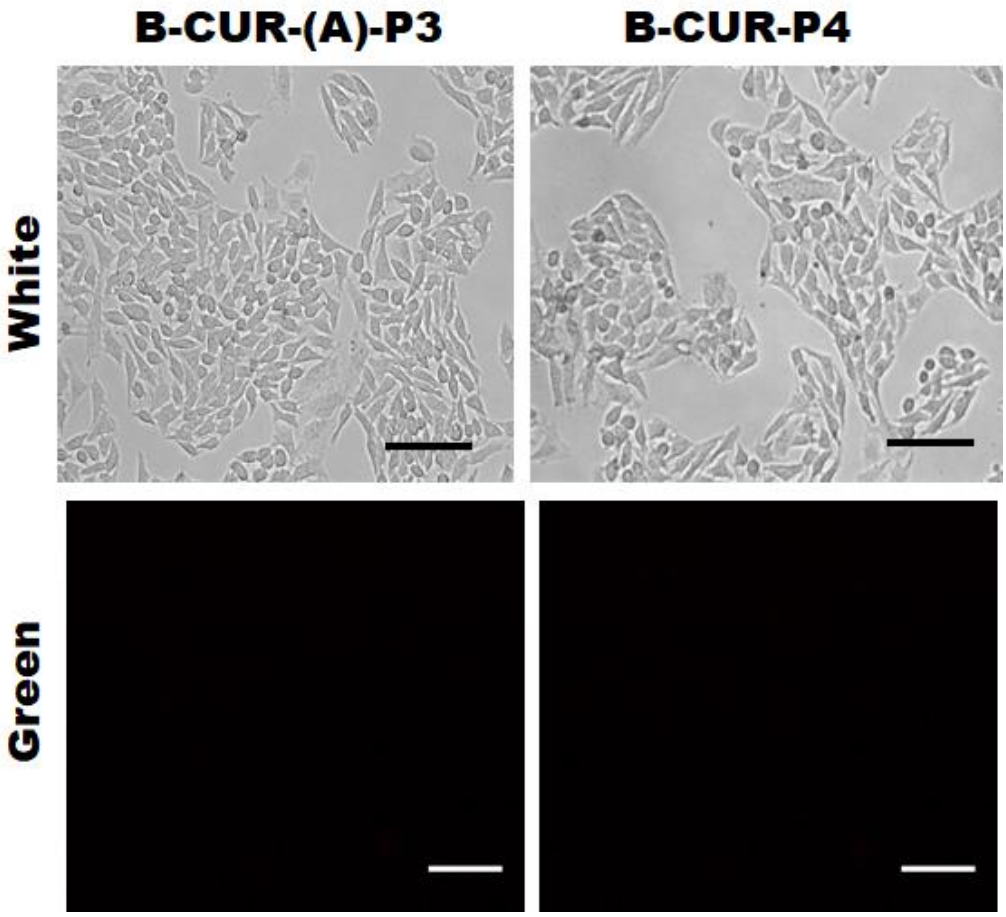

Figure 5.21: Comparison of cellular internalization of responsive and non-responsive micelles on NIH3T3 cell lines (Scale 1.0 µm, 40 X magnification)

For the confirmation of receptor mediated internalization of carriers likewise performed in MTT assay, the cellular internalization was also carried out in the presence of 1 mg/ml of free biotin **(as shown in figure 5.22)**. There is comparatively less fluorescence observed in these cells that is due to hindered internalization due to interference of free biotin.

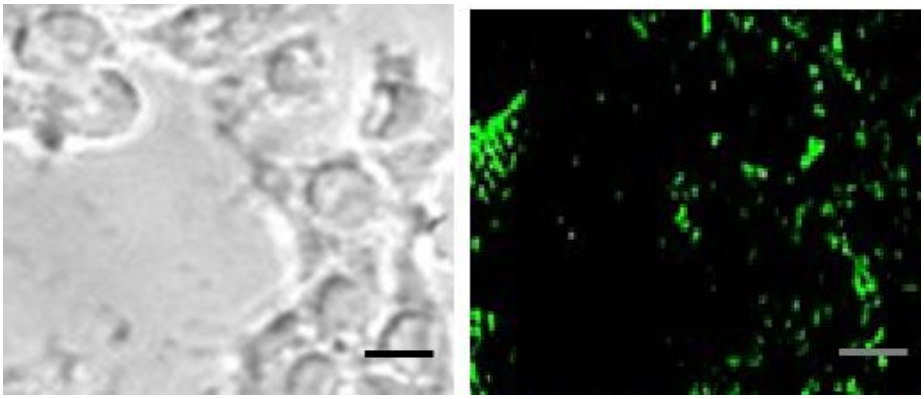

Figure 5.22: Cellular internalization of from fluorescein B-CUR-(A)-P3 on the HepG2 cell lines pretreated with 1 mg/ml of biotin

The PI staining studies further provide corroborative evidences of the efficiency of micelles in inducing cytotoxic effect to cancer cells. **Figure 5.20B** indicated no cell death upon dosage with blank micelles. However an evident cytotoxicity was observed on dosing the DOX loaded micelles. Since **B-CUR-P4** is non-responsive, it is not able to deliver the loaded cargo of drug to the cancer site even after being internalized and hence fail to exert an effective anticancer effect. This proves the significance of introducing acid labile acetal and enzyme responsive ester linkage for an effective drug delivery and cancer elimination.

5.3.7 Assessment of the efficacy of self-therapeutic micelles as drug delivery system for anti-cancer effect in vivo

Since amongst all the responsive carriers DOX loaded B-CUR-(A)-P3 demonstrated the most effective internalization and cytotoxic effect; it was further subjected to in-vivo evaluation. Its performance for cancer management was compared with the nonresponsive DOX loaded B-CUR-P4. For the experiment, animals were divided in 7 treatment groups as follows with n=6 mice per group. The animals in group 1(G1) were dosed only with double distilled water and designated as control group. The physiological parameters determined from this group were considered as the standard values for cancer free condition. The animals in the remaining groups (G2 to G7) were administered with HEPG2 cells intraperitoneally to induce hepatic tumor

(HCC). After the successful tumor induction, animals of group 2 (G2) were dosed with only PBS and designated as untreated group. The treatment groups consisted of group 3 (G3) dosed only with DOX, group 4 (G4) dosed with B-CUR-(A)-P3, group 5 (G5) injected with B-CUR-P4, group 6 (G6) administered with DOX loaded B-CUR-(A)-P3 (10 mg kg^{-1}) and group 7 (G7) treated with DOX loaded B-CUR-P4.

The analysis of changes in body weight as shown in **figure 5.23A** shows a drastic decrease in the body weight of G2 mice as compared to G1 that is due to cancer development. The mice in and G5 showed weight similar to G2 mice indicated that the non-response nanocarriers don't exert any effect on the growth of tumor. However, G4 mice also demonstrated weight similar to those of G1. This signifies that the micelles are able to undergo enzyme responsive cleavage causing the release of curcumin, which induces cytotoxicity to cancer cells due to treatment. Amongst the two DOX loaded carriers groups, i.e. G6 and G7, G6 was found to show a remarkable weight reduction (compared to untreated G2) and attain a weight similar to mice in control G1. Similar observations were seen when the liver weights **(figure 5.23B)** were analyzed.

The detailed study of liver indices (SGOT, SGPT) **(figure 5.23C & D)** corroborates with the observations of liver and body weight analysis. With mice in G4 and G6 showing the most effective response to treatment. For investigation of the effective drug release at tumor site by the micelles, metallopeptidase (MMP) concentration in blood serum was also carried out.

The level of MMP-9, a biomarker associated with invasiveness and metastasis of cancer was analyzed in all the treatment groups **(figure 5.24A)**. Since G1 is a non-cancer group, it shows low levels of MMP which is an indication of no cancer progression. G2 shows highly elated level of MMP-9, >800 ng/ml concentration. G4 group shows a drop in the level ~ 300 ng/ml that and in G6 the level further drops <100 ng/ml. Similar observations were obtained when a hepatocellular carcinoma specific α-fetoprotein (AFP) was quantitatively analyzed following the treatment regimen [29]. A drastic reduction in the AFP concentration was found in G4 and G6 mice **(figure 5.24B)**. The histoarchitechture of the liver tissue as observed post hematoxylin and eosin staining of tumor tissue in all the groups are shown in **figure 5.24C**. The untreated groupG2 showed predominant areas of tumor infiltration and showed severe mitoses and pleomorphic nuclei. However in groups G4 and G6 the tissues showed necrosis areas stained by eosin [30].

These findings led to the conclusion that the responsive micelle containing esterase labile curcumin as a prodrug has the ability to act as a self-therapeutic system in tumor microenvironment. The anticancer effect of these prodrug micelles was further enhanced upon DOX loading making the carrier more aggressive towards cancer treatment.

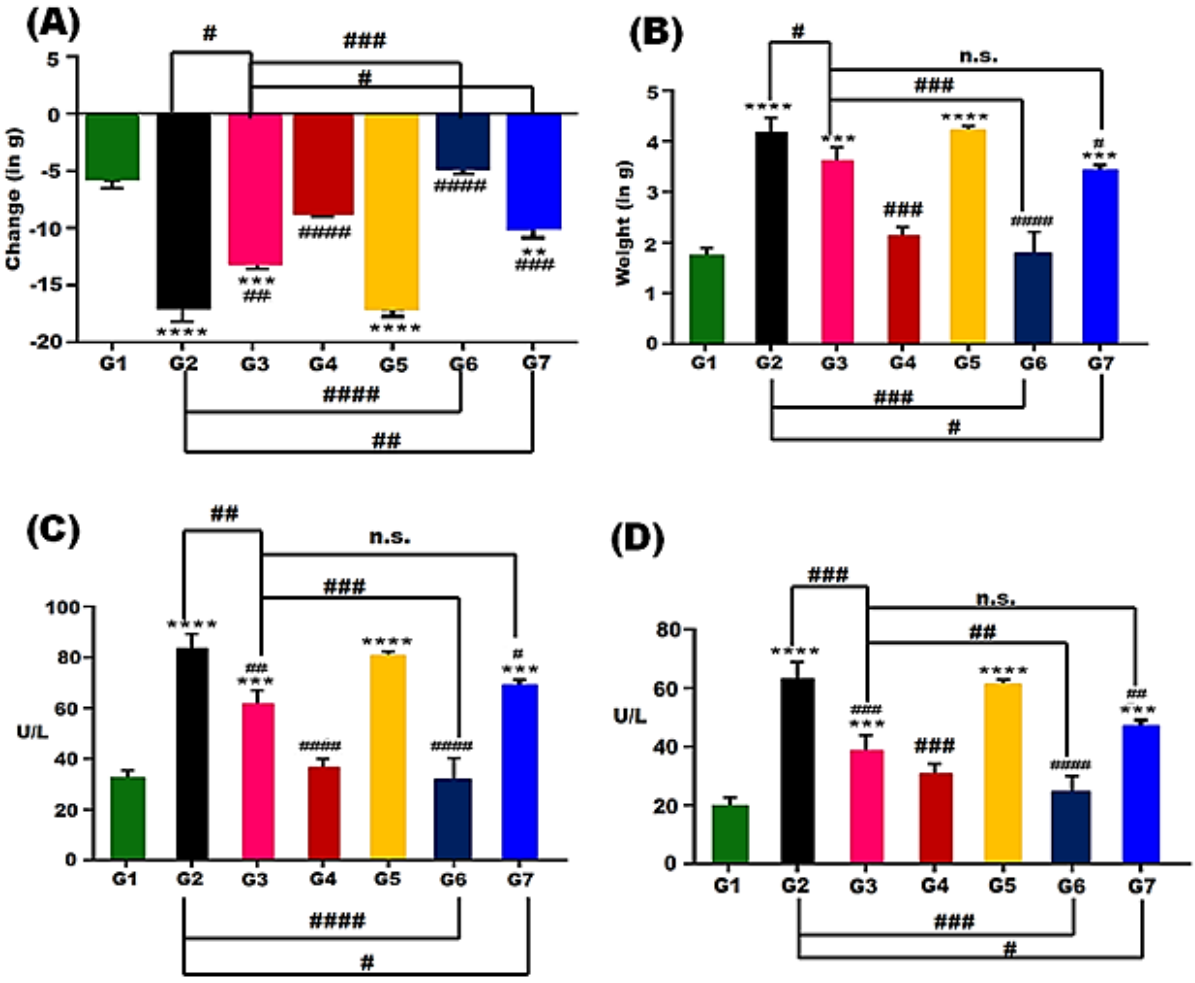

Figure 5.23: Comparison of (A) mice body weight (B) liver weight and liver indices (C) SGOT, (D) SGPT in various treatment groups.

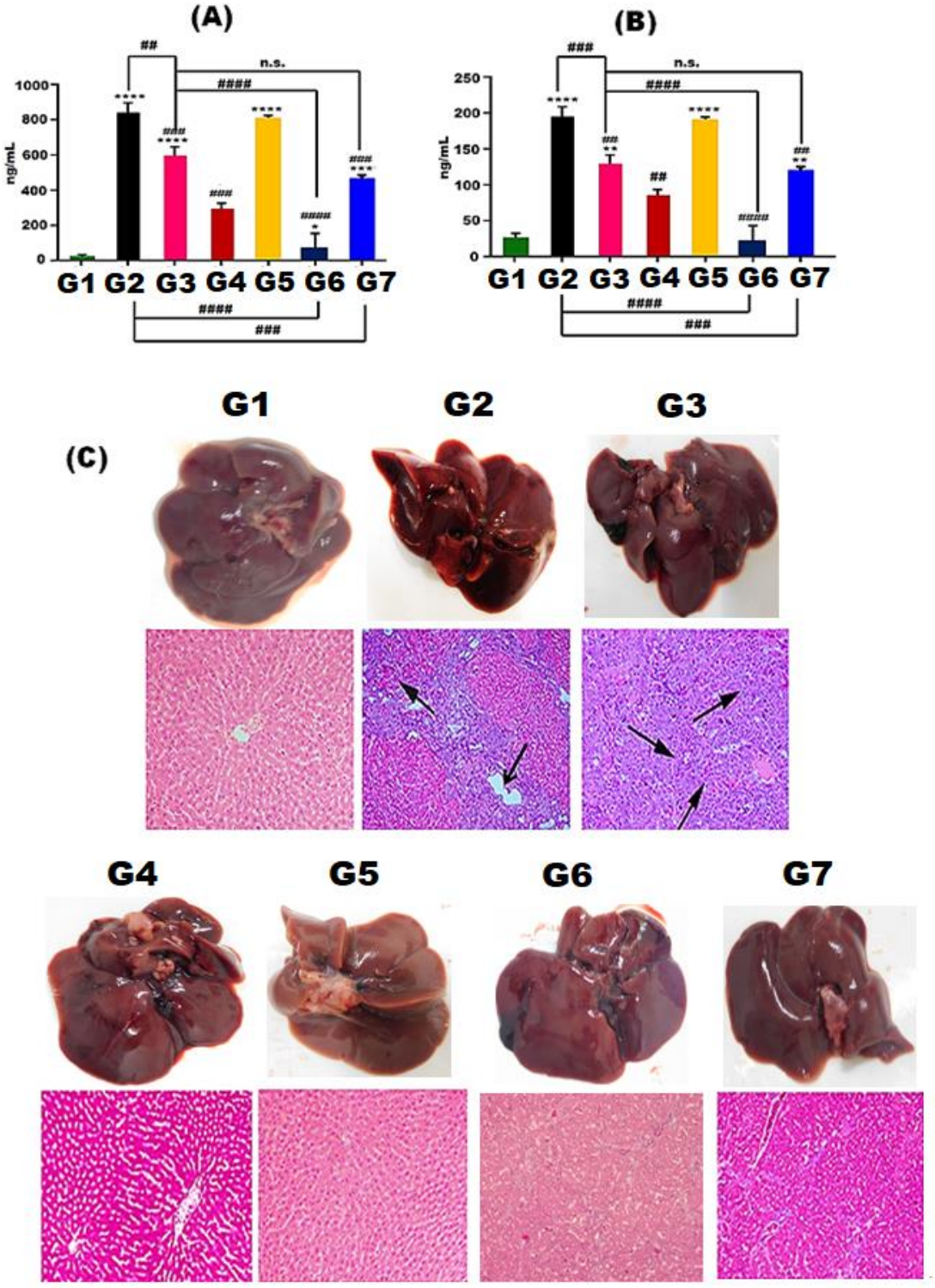

Figure 5.24: Comparison of markers of tumor progression (A) MMP-9 and (B) AFP in the mice of various treatment groups. (C) Histoarchitechture of liver tissues post H&E staining (Scale: 1 µm)

5.3.8 Mechanism of action of pro-drug micelles as devised from analytical and pre-clinical evaluations

The pH, enzyme dual-responsive curcumin pro-drug micelles are primarily composed of two individual fragments as per the schematic illustration show in **figure 5.25**. First component is a P-gp inhibitor; curcumin infused as a part of the polymer by an enzyme sensitive functionality. Second component is the neoplastic agent doxorubicin, that is housed in the hydrophobic interior of the micelles containing, acid responsive acetal linkages. Upon the intravenous injection of these micelles in the blood stream, the carriers internalize selectively only in the cancer cells via a receptor mediated endocytosis. Since the surface of HepG2 cells possess biotin receptors, the carriers can readily infiltrate the tumor and accumulate therein. In the tumor microenvironment, due to the presence of relatively acidic environment, the acetal linkage undergoes hydrolysis causing the first disassembly of the micelle, releasing entrapped DOX and curcumin in its prodrug form.

A second disassembly occurs when the enzyme linkage that binds curcumin with its pro-moiety undergoes cleavage under the influence of intracellular lysosomal enzymes further accelerating intracellular drug delivery. This hypothesis corroborates with results of various physicochemical parameters studied for various micellar formulations. Further the results of in-vitro drug release, cellular internalization and PI staining assisted cellular toxicity studies also support the theory of biotin mediated internalization and stimuli responsive drug release. A combination index of less than 1 further proved that cocktail chemotherapy works synergistically for tumor regression as observed from in-vivo studies on HCC induced nude mice model.

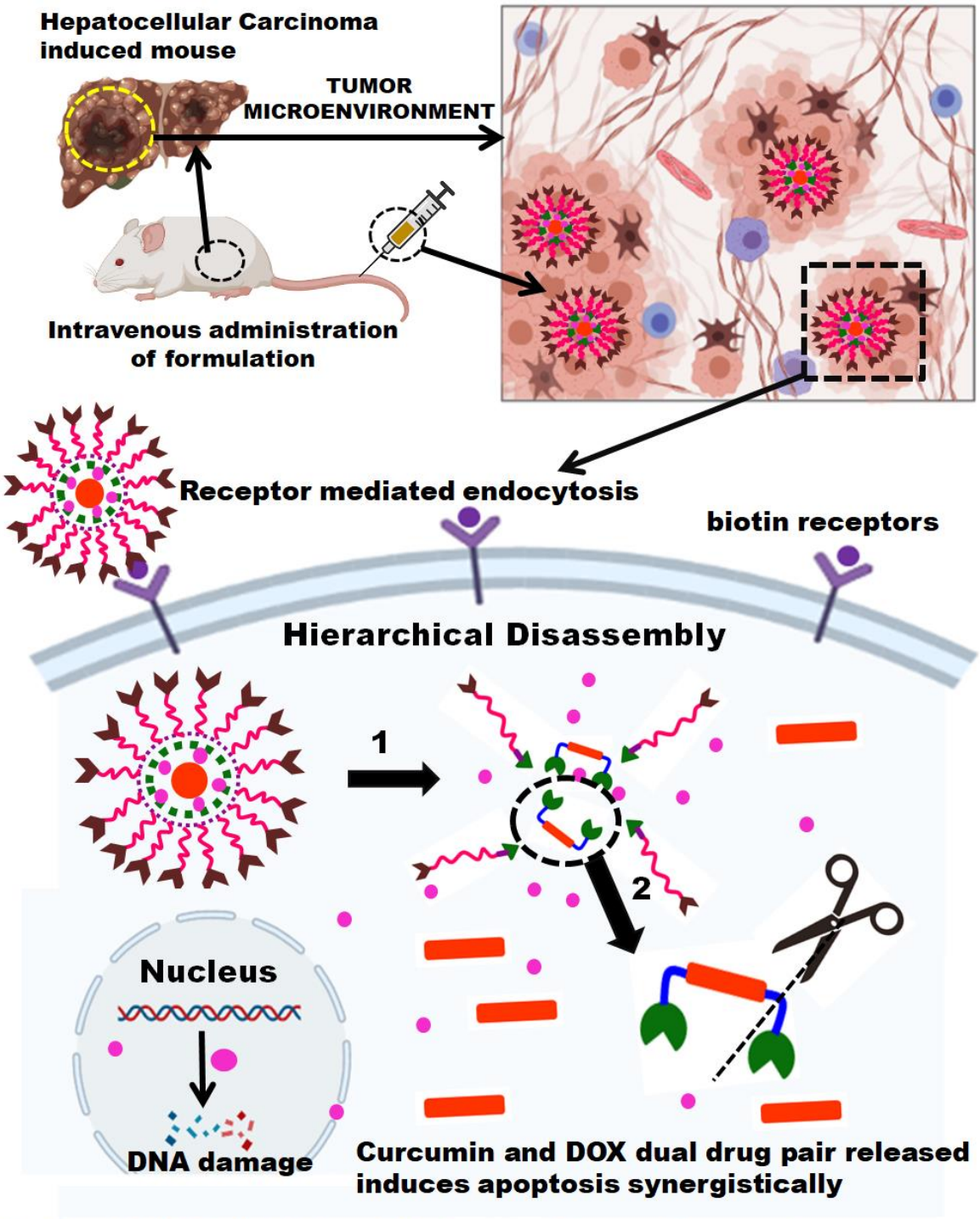

Figure 5.25: Schematic illustration of dual-responsive curcumin prodrug micelle undergoing hierarchical disassembly. The micelles were constructed with enzyme cleavable curcumin prodrug units and acid responsive acetal linkages and encapsulated with DOX.

5.4 Conclusion

To summarize, this work reports the synthesis of acetal and ester linkages containing curcumin derived block co-polymeric prodrug micelles capable of sequential degradation in tumor microenvironment. The carriers are non-toxic to normal cell lines and exert an anticancer effect on cancerous HepG2 cell lines. The micelles have sizes in the range of 150-250 nm and possess suitably low CMC values to exhibit good stability. The micelles demonstrated 63 % entrapment efficiency for DOX. The DOX release occurs under mild intracellular acidic media of cancer cells due to the acetal hydrolysis in these conditions. Further the curcumin release occurs upon enzymatic cleavage of ester linkage in the polymer structure. The micelles were found to rupture and release >80% of both DOX and curcumin on exposure to tumor milieu of low pH and lysosomal esterase enzyme. The CI calculated on the HepG2 cell lines was found to be <1 hence the neoplastic drug DOX and P-gp inhibitor curcumin are found to act synergistically for apoptosis of cancer cells. These biotin tagged polymeric nanocarriers can selectively target cancer cells via receptor mediated endocytosis that has been proved from MTT assay and cellular internalization experiments on biotin pre-treated HepG2 cell lines. The PI staining cytotoxicity studies also showed cell death post effective cellular internalization. The non-responsive micelle was found to be much less selective and less efficient for drug delivery. The in-vivo studies performed on nude mice, corroborated with the in-vitro observations. Drastically low levels of cancer specific biomarkers like MMP-9 and AFP upon treatment with responsive blank micelle support the hypothesis that the synthesized micelles are potentially self-therapeutic in nature. The loading of DOX further makes the carrier more aggressive for tumor regression.

5.5 References

1. Ang CY, Tan SY, Zhao Y. *Org Biomol Chem*. 2014; 12: 4776–4806.
2. Sun X, Zhang J, Yang C, Huang Z, Shi M, Pan S, Hu H, Qiao M, Chen D, Zhao X. *ACS Appl Mater Interfaces*. 2019; 11: 11865–11875.
3. Dai YD, Sun XY, Sun W, Yang JB, Liu R, Luo Y, Zhang T, Tian Y, Lu ZL, He L. *Org Biomol Chem*. 2019; 17: 5570–5577.
4. Li J, Zhang L, Lin Y, Xiao H, Zuo M, Cheng D, Shuai X. *RSC Adv*. 2016; 6: 9160–9163.
5. Palamoor M, Jablonski MM. *Mol Pharm*. 2013; 10: 701–708.
6. Sonawane SJ, Kalhapure RS, Govender T. *Eur J Pharm Sci*. 2017; 99: 45–65.

7. Li N, Lu W, Yu J, Xiao Y, Liu S, Gan L, Huang J. *Mater Sci Eng C*. 2018; 91: 179–189.
8. Huang F, Cheng R, Meng F, Deng C, Zhong Z. *Biomacromolecules*. 2015; 16: 2228–2236.
9. Wan D, Li C, Pan J. *ACS Appl Bio Mater*. 2020.
10. Hiruta Y, Kanda Y, Katsuyama N, Kanazawa H. *RSC Adv*. 2017; 7: 29540–29549.
11. Yang X, Grailer JJ, Rowland IJ, Javadi A, Hurley SA, Matson VZ, Steeber DA, Gong S. *ACS Nano*. 2010; 4: 6805–6817.
12. Ghosh R, Dey J. *Langmuir*. 2020; 36: 5829–5838.
13. Nanayakkara AK, Follit CA, Chen G, Williams NS, Vogel PD, Wise JG. *Sci Rep*. 2018; 8: 1–18.
14. Joshi P, Singh S, Wani A, Sharma S, Jain SK, Singh B, Gupta BD, Satti NK, Koul S, Khan IA, Kumar A, Bharate SB, Vishwakarma RA. *Medchemcomm*. 2014; 5: 1540–1547.
15. Sagnou M, Novikov FN, Ivanova ES, Alexiou P, Stroylov VS, Titov IY, Tatarskiy V V., Vagida MS, Pelecanou M, Shtil AA, Chilov GG. *Eur J Med Chem*. 2020; 198: 112331.
16. Yang W, Cheng Y, Xu T, Wang X, Wen L ping. *Eur J Med Chem*. 2009; 44: 862–868.
17. Park S, Kim E, Kim WY, Kang C, Kim JS. *Chem Commun*. 2015; 51: 9343–9345.
18. Roughley PJ, Whiting DA. *JCS Perkin I*. 1973: 2379–2388.
19. Zhao Y, Zhao J, Hao C, Han M, Wang M, Guo Y, Wang X. *RSC Adv*. 2016; 6: 2602–2610.
20. Zhong Y, Yang W, Sun H, Cheng R, Meng F, Deng C, Zhong Z. *Biomacromolecules*. 2013; 14: 3723–3730.
21. Zhang Z, Chen X, Gao X, Yao X, Chen L, He C, Chen X. *RSC Adv*. 2015; 5: 18593–18600.
22. Dutta B, Barick KC, Verma G, Aswal VK, Freilich I, Danino D, Singh BG, Priyadarsini KI, Hassan PA. *Phys Chem Chem Phys*. 2017; 19: 26821–26832.
23. Gillies ER, Goodwin AP, Fréchet JMJ. *Bioconjug Chem*. 2004; 15: 1254–1263.
24. Sill KN, Sullivan B, Carie A, Edward Semple J. *Biomacromolecules*. 2017; 18: 1874–1884.
25. Qu JB, Chapman R, Chen F, Lu H, Stenzel MH. *ACS Appl Mater Interfaces*. 2017; 9: 13865–13874.
26. Li R, Peng F, Cai J, Yang D, Zhang P. *Asian J Pharm Sci*. 2020; 15: 311–325.

27. Deshpande NU, Jayakannan M. *Biomacromolecules*. 2018; 19: 3572–3585.
28. Das M, Nariya P, Joshi A, Vohra A, Devkar R. *Carbohydr Polym*. 2020; 247: 116751.
29. Isaacson KJ, Jensen MM, Subrahmanyam NB, City SL, Chemistry P, City SL, City SL. *J Control Release*. 2018; 10: 62–75.
30. Chithrani BD, Ghazani AA, Chan WCW. *Nano Lett*. 2006; 6: 662–668.